1Induced ligno-suberin vascular coating and tyramine-derived hydroxycinnamic acid amides restrict *Ralstonia solanacearum* colonization in resistant tomato

Short title: A pathogen-induced ligno-suberin vascular coating

Anurag Kashyap[1,¥], Álvaro Luis Jiménez-Jiménez[1,#], Weiqi Zhang[1,#], Montserrat Capellades[1,2], Sumithra Srinivasan[3], Anna Laromaine[3], Olga Serra[4], Mercè Figueras[4], Jorge Rencoret[5], Ana Gutiérrez[5], Marc Valls[1,6], Nuria S. Coll[1,2,*]

[1] Centre for Research in Agricultural Genomics (CRAG), CSIC-IRTA-UAB-UB, Campus UAB, 08193 Bellaterra, Spain

[2] Consejo Superior de Investigaciones Científicas (CSIC), 08001 Barcelona, Spain

[3] Institute of Material Science of Barcelona (ICMAB), CSIC, Campus UAB, 08193 Bellaterra, Spain

[4] Laboratori del Suro, Biology Department, Universitat de Girona, Campus Montilivi, 17003 Girona, Spain

[5] Institute of Natural Resources and Agrobiology of Seville (IRNAS), CSIC, 41012 Seville, Spain

[6] Department of Genetics, Universitat de Barcelona, 08028 Barcelona, Spain

[#] These authors contributed equally to the work

[*] Author for correspondence: Nuria S. Coll. e-mail: nuria.sanchez-coll@cragenomica.es

Total word count: 6806

Word count Introduction: 1063

Word count Materials and Methods: 1244

Word count Results: 2490

Word count Discussion: 2009

Number of figures: 9 (1, 2, 3, 4, 5, 7, 8, 9 in color)

Supporting information is included

ORCID AUTHORS:

Anurag Kashyap 0000-0003-2622-8209
Álvaro Jiménez-Jiménez 0000-0002-9406-4595
Weiqi Zhang 0000-0002-2535-1398
Montse Capellades 0000-0001-9514-2885
Sumithra Srinivasan 0000-0002-0473-9801
Anna Laromaine 0000-0002-4764-0780
Olga Serra 0000-0002-1678-0932
Mercè Figueras 0000-0002-6288-1830
Jorge Rencoret 0000-0003-2728-7331
Ana Gutiérrez 0000-0002-8823-9029
Marc Valls 0000-0003-2312-0091
Núria S. Coll 0000-0002-8889-0399

TWITTER ACCOUNTS:
@BactoDeath
@anuragkashyap11
@cork_lab
@alaromaine
@RencoretJorge
@sumithrayasaswi

Summary

- Tomato varieties resistant to the bacterial wilt pathogen *Ralstonia solanacearum* have the ability to restrict bacterial movement in the plant. Inducible vascular cell wall reinforcements seem to play a key role in confining *R. solanacearum* into the xylem vasculature of resistant tomato. However, the type of compounds involved in such vascular physico-chemical barriers remain understudied, while being a key component of resistance.
- Here we use a combination of histological and live-imaging techniques, together with spectroscopy and gene expression analysis to understand the nature of *R. solanacearum*-induced formation of vascular coatings in resistant tomato.
- We describe that resistant tomato specifically responds to infection by assembling a vascular structural barrier formed by a ligno-suberin coating and tyramine-derived hydroxycinnamic acid amides. Further, we show that overexpressing genes of the ligno-suberin pathway in a commercial susceptible variety of tomato restricts *R. solanacearum* movement inside the plant and slows disease progression, enhancing resistance to the pathogen.
- We propose that the induced barrier in resistant plants does not only restrict the movement of the pathogen, but may also prevent cell wall degradation by the pathogen and confer anti-microbial properties, effectively contributing to resistance.

Key words:

Bacterial wilt, Feruloyltyramine, HCAAs, Lignin, *Ralstonia solanacearum*, Suberin, Tomato, Vascular coating

Introduction

In natural environments plants are constantly exposed to diverse microbiota, including pathogenic organisms. In addition to pre-existing structural cell barriers that act as a first line of defense (Serrano *et al*., 2014; Falter *et al*., 2015), pathogen perception results in activation of a complex, multi-layered immune system in plants (Jones and Dangl, 2006). As part of the suite of inducible defenses, *de novo* formation of physico-chemical barriers prevents pathogen colonization and spread inside the plant. Despite their importance, the exact composition of these barriers, as well as the mechanisms that lead to their formation in the plant upon pathogen invasion remain largely unknown.

The interaction between the soil-borne bacterial wilt pathogen *Ralstonia solanacearum* and tomato offers a paradigmatic scenario to study inducible physico-chemical barriers, because of its agro-economic impact, and the well-developed genetic and molecular tools available in both organisms. *R. solanacearum* enters the root system through wounds or at the points of emergence of lateral roots, where the epidermal and endodermal barriers may be compromised (Vasse *et al*., 1995; Álvarez *et al*., 2010; Ursache *et al*., 2021). After entering the root, the bacterium moves centripetally towards the vasculature and once it reaches the xylem, it multiplies and spreads vertically within the vessels and horizontally to other vessels and the surrounding tissues (Digonnet *et al*., 2012).

The xylem tissue is a major battleground for the interaction between vascular wilt pathogens and their hosts, where the outcome of the infection is at stake (Yadeta and Thomma, 2013). To prevent the spread of pathogenic propagules, the xylem vasculature of resistant plants undergoes intense structural and metabolic modifications, such as reinforcing the walls of xylem vessels, pit membranes and surrounding xylem parenchyma cells in response to pathogens (Street *et al*., 1986; Benhamou, 1995). This prevents pathogen colonization of the surrounding parenchyma cells, nearby vessels and inter-cellular spaces through degeneration of the vessel pit membranes or cell walls by the pathogen (Nakaho *et al*., 2000; Digonnet *et al*., 2012; Liu *et al*., 2005; Pérez-Donoso *et al*., 2010; Lowe-Power *et al*., 2018). This vascular confinement is an effective strategy

commonly found among plants resistant to vascular wilt pathogens such as *R. solanacearum,* which otherwise spread systemically and eventually kill the plant (McGarvey et al., 1999; Vasse et al., 2000; Potter *et al*., 2011; Caldwell et al., 2017; Scortichini, 2020; Kashyap *et al*., 2021).

Among the various tomato germplasms, the cultivar Hawaii 7996 (H7996) is the most effective natural source of resistance against *R. solanacearum* (Nakaho *et al*., 2004; Grimault *et al*., 1994). In this cultivar, resistance to *R. solanacearum* is a complex polygenic trait (2000; Thoquet *et al*., 1996; Mangin *et al*., 1999; Wang *et al*., 2013). Our previous study identified the bottlenecks through which H7996 is able to limit *R. solanacearum* spread *in planta* (Planas-Marquès *et al*., 2019), namely: i) root colonization, ii) vertical movement from roots to shoots, iii) circular invasion of the vascular bundle and iv) radial apoplastic spread from the vessels into the cortex. Vascular cell wall reinforcements seem to play a key role in confining *R. solanacearum* into the xylem vascular bundles of resistant tomato H7996. Ultra-microscopic studies in resistant tomato showed that the pit membranes, as well as xylem vessel walls and parenchyma cells form a conspicuously thick coating in the form of an electron dense amorphous layer, as part of the defense response against *R. solanacearum* (Nakaho *et al*., 2000; Kim *et al*., 2016;).

Among the polymers constituting vascular coating structures, lignin is the most typically found, constituting an integral part of the secondary cell wall of the xylem vasculature. Lignin is well documented as a common structural defense against vascular wilt pathogens (Novo *et al*., 2017; Zeiss et al., 2019; Kashyap *et al*., 2021) and it is also emerging as an important inducible defense component in other diseases/pests affecting the vasculature (Jhu et al., 2021; Joo et al., 2021) Suberin has also been reported to be deposited in vascular coatings as a defense response (Kashyap *et al*., 2021), although the mechanisms regulating its synthesis, spatio-temporal dynamics and inducibility remain elusive. Interestingly, root microbiota has been recently shown to shape suberin deposits in the plant, highlighting its central role in plant-microbe interactions (Salas-González *et al*., 2021). Suberin is a polyester containing long and very long chain fatty acids and derivatives and also some aromatics, mainly ferulic acid. Cells that accumulate suberin also accumulate lignin, whose

deposition has been described to precede that of suberin in phellem cells (Lulai and Corsini, 1998). This lignin is also known as a lignin-like polymer, which consists of hydroxycinnamates and monolignols (Graça, 2015). The ligno-suberin heteropolymer formed by the lignin-like polymer and suberin has been also referred to as the poly(aromatic) and poly(aliphatic) domains of suberin, respectively. Commonly, suberized cell walls also comprise soluble phenolic compounds, which share biosynthetic pathways with suberin and lignin (Bernards, 2002).

Ferulic acid present in the suberin and lignin-like fractions is proposed to link both polymers (Graça, 2010) and its continuous production has been demonstrated essential for suberin deposition (Andersen *et al*., 2021). Ferulic acid amides, such as feruloyltyramine and feruloyloctopamine, have been described as structural components of the lignin-like polymer and in the phenolic soluble fraction of suberizing wound-healing potato tuber (Negrel *et al*., 1996; Razem and Bernards, 2002). Ferulic acid amides belong to the Hydroxycinnamic acid amide (HCAA) family, which present antimicrobial activity and are considered biomarkers during plant-pathogen interactions (Zeiss *et al*., 2021). However, the precise role of HCAAs in plant defense remains to be elucidated (Macoy *et al*., 2015). Besides their direct antimicrobial activity as soluble phenols, HCAAs have also been proposed to cross-link to cell wall structural polymers during infection, potentially contributing towards the formation of a phenolic barrier that can make the cell wall resilient to pathogenic degradation (Zeiss *et al*., 2021).

In the present study, we conducted a detailed investigation of the inducibility, structure and composition of the xylem vascular wall reinforcements that restrict *R. solanacerum* colonization in resistant tomato. Using a combination of histological and live-imaging techniques, together with spectroscopy and gene expression analysis we provide important new insights into the pathogen-induced formation of vascular coatings. In particular, we show that a ligno-suberin vascular coating and tyramine-derived HCAAs contribute to restriction of *R. solanacearum* in resistant tomato. In addition, we demonstrate that genes in the ligno-suberin-associated pathways can be explored to engineer resistance against *R. solanacearum* into commercial susceptible varieties of tomato.

Materials and Methods

Plant materials and growth conditions

Tomato (*Solanum lycopersicum*) varieties Marmande, Hawaii 7996 (H7996) and Moneymaker (wild-type and *35S::THT 1-3,* generated by Campos *et al.*, (2014)), were used. Plants were grown in controlled growth chambers at 60% humidity, 12 h day/night and 27ºC (LED lighting) or 25ºC (fluorescent lighting).

Ralstonia solanacearum strains and growth conditions

R. solanacearum GMI1000 strain (Phylotype I, race 1 biovar 3) was used, including luminescent and fluorescent reporter strains of *R. solanacearum* GMI1000 described in (Cruz *et al*., 2014; Planas-Marquès *et al*., 2019).

Cloning and stable transformation in tomato

For generation of the *35S::FHT-HA* construct the *FHT* (Solyc03g097500) coding sequence was amplified from tomato H7996 cDNA using the forward and reverse primers part7FHTF1 and part7FHTHAR1, respectively (Table S1). The amplified product was cloned into the pJET1.2/blunt cloning vector using CloneJet PCR cloning kit (Thermofisher) and then digested by *Sma*I and *Bam*HI. The digested products were purified using NZYGelpure (Nzytech) followed by ligation into the pART7 and later to pART27 vector (Gleave, 1992). pART27 containing *35S::FHT-HA* was transformed into Marmande. For this, the construct was transformed into *Agrobacterium tumefaciens* strain C58C1. Cotyledon explant preparation, selection, and regeneration followed the methods described by (Mazier *et al*., 2011). Transformants were selected on kanamycin-containing medium. Accumulation of FHT-HA protein was assayed by immunoblot with a monoclonal HA antibody (GenScript).

Bacterial inoculation in plants

Four to five week-old tomato plants were inoculated through roots with *R. solanacearum* using the soil drenching method with a to $1x10^7$ CFU ml^{-1} suspension of bacteria as

described in (Planas-Marquès *et al*., 2018). Inoculated plants were kept in a growth chamber at 27°C. For tomato leaf infiltration, plants were vacuum-infiltrated by submerging the whole aerial part in a ~10^5 CFU ml^{-1} bacterial suspension as described in Planas-Marquès *et al.*, (2018). For inoculation directly onto the stem vasculature, 10 µl (5 µl at a time) of 10^5 CFU ml^{-1} bacterial suspension was placed at the node of the petiole and pin-inoculated using a sterile needle (30G×½″, BD Microlance, Becton Dickinson).

R. solanacearum* pathogenicity assays and quantification of bacterial growth *in planta

Infected plants were scored for wilting symptoms using a scale from 0 to 4: 0=healthy plant with no wilt, 1=25%, 2=50%, 3=75%, and 4=100% of the canopy wilted as described by Planas-Marquès *et al.*, (2019). The relative light units per second ($RLU \cdot s^{-1}$) readings were converted to $CFU \cdot g^{-1}$ tissue as described in Planas-Marquès *et al.*, (2019). For bacterial colonization assays using GFP reporter strain, transverse stem cross-sections were made at the inoculation point and at a distance of 0.5 cm, 1 cm, 2 cm and 3 cm in both upward and downward direction, using a sterile razor blade. Quantification of mean green fluorescence was done using ImageJ software (Planas-Marquès *et al*., 2019). For leaf *in planta* multiplication assays, 3 leaf discs of 0.8 cm^2 were homogenized in 200 µl of sterile distilled water. CFU cm^{-2} leaf tissue were calculated after dilution plating of samples with appropriate selection antibiotics and CFU counting 24 hours later.

Histological methods

Thin (approximately 150 µm) transverse cross-sections were obtained with a sterile razor blade from a 1.5 cm area of the taproot-to-hypocotyl transition zone located immediately below the soil line (Fig. S1a). Inoculated plants were sectioned when bacterial colonization level reached 10^5 CFU g^{-1} taproot-to-hypocotyl transition zone tissue. This corresponded to 4 dpi in Marmande and 9 dpi in H7996, at which stage only H7996 sections showed a localized browning at one xylem pole indicative of infection. Sections were kept in 70 % ethanol at room temperature for 5 days and examined using fluorescence microscopy using a Leica DM6B-Z microscope under UV illumination (340-380 nm excitation and 410-450 nm barrier filters). Autofluorescence emitted from phenolic deposits was recorded using a Leica-DFC9000GT-VSC07341 camera and the signal was pseudo-colored green. Sections

were also stained with Phloroglucinol-HCl for the detection of lignin and observed under bright field (Pomar *et al*., 2004). Photographs were taken with a DP71 Olympus digital camera. Cross-sections were also observed under UV with a Leica-DM6B-Z microscope (340-380 nm excitation and 410-450 nm barrier filters). To detect the autofluoresecent blue-to-green pH-dependent color conversion of wall-bound ferulic acid cross-sections were first mounted in 70% ethanol (neutral pH) and then in 1N KOH (pH above 10) adapting the protocol from (Harris and Trethewey, 2010; Carnachan and Harris, 2000; Donaldson and Williams, 2018). A Leica DM6B-Z microscope was used to observe autofluorescence (340-380 nm excitation and 410-450 nm barrier filters). Images were recorded using a Leica MC190-HD-0518131623 digital camera. To visualize suberin aliphatics, sections were treated with 5 % Sudan IV, dissolved in 70 % ethanol and illuminated with UV light. These sections were subsequently treated with 1N KOH to detect ferulic acid as described above. For both ferulic acid and suberin, the HC PL APO or HC PL FLUOTAR objectives of the Leica DM6B-Z microscope were used and images were captured using a Leica MC190-HD-0518131623 color digital camera. The UV autofluorescence signal from xylem vessel walls and surrounding layers was measured using the LAS X Leica software and changes in ferulate accumulation were quantified using ImageJ software by selecting the area of xylem vessel walls showing autoflorescence. Quantifications of fluorescence intensity were normalized per µm of region of interest (ROI), which corresponded to a particular area of the vascular bundles, where main vessels concentrate (represented in Fig. 1b). Basically the line is drawn at each of the 4 corners in the whole image and then the fluorescence is normalized by the length of the lines.

2D-NMR

The samples of a pool of 15 tomato plants (taproot-to-hypocotyl region), water treated or having a bacterial load of 10^5 CFU.g^{-1} were milled and extracted sequentially with water, 80% ethanol, and with acetone, by sonicating in an ultrasonic bath during 30 min each time, centrifuging and eliminating the supernatant. Then, lignin/suberin fraction was enzymatically isolated by hydrolyzing the carbohydrates fraction with Cellulysin (Calbiochem), as previously described (Rico *et al*. 2014). Approximately 20 mg of enzymatic lignin/suberin preparation was dissolved in 0.6 mL of DMSO-d_6. Heteronuclear

single quantum coherence (HSQC) spectra were acquired on a Bruker AVANCE III 500 MHz spectrometer equipped with a 5 mm TCI cryoprobe, using the experimental conditions previously described (Rico *et al*., 2014). HSQC cross-signals were assigned and quantified as described (Rencoret *et al*., 2018; del Río *et al*., 2018; Mahmoud *et al*., 2020). In the aromatic region, the correlation signals of G_2 and $S_{2,6}$ were used to estimate the content of the respective G- and S-lignin units. The C_α/H_α signals of the β–*O*–4′ ethers (A_α), phenylcoumarans (B_α), and resinols (C_α) in the linkages region were used to estimate their relative abundances, whereas the C_γ/H_γ signal was used in the case of cinnamyl alcohol end-units (I_γ).

RNA extraction, **cDNA synthesis and quantitative RT-PCR analysis**

Taproot-to-hypocotyl transition zone sections of ~ 0.5 mm thickness were obtained and the xylem vascular tissues (vascular bundles and surrounding parenchyma cells) were collected and kept in liquid nitrogen. Each sample comprised taproot-to-hypocotyl transition zone xylem tissues of 6 plants. RNA was extracted using the Maxwell RSC Plant RNA Kit (Promega). cDNA was synthesized from 2 µg RNA using High Capacity cDNA Reverse Transcription Kit (Applied Biosystems, USA). cDNA amplification and analysis was performed using the LightCycler 480 System (Roche). The Elongation Factor 1 alpha housekeeping gene (*eEF1 α, Solyc06g005060*) was used as a reference. All reactions were run in triplicate for each biological replicates. Melting curves and relative quantification of target genes were determined using the software LightCycler V1.5 (Roche). The level of expression relative to the reference gene was calculated using the formula $2^{-\Delta CT}$, where ΔCT = (CT RNA target - CT reference RNA).

Statistical analysis

Statistical analyses were performed using Statgraphics software. All statistical tests are indicated in the respective figure legends.

Results:

Resistant H7996 tomato restricts *R. solanacearum* colonization and induces a vascular coating response involving wall-bound phenolics

In order to understand the mechanisms underscoring restriction of *R. solanacearum* spread in resistant tomato varieties we used the resistant variety Hawaii 7996 (H7996) and compared it to the susceptible cultivar Marmande. In our assay conditions, most Marmande plants were wilted 10 days after inoculation with *R. solanacearum* GMI1000, while H7996 plants remained largely asymptomatic (Fig. 1a, S2a and (Planas-Marquès *et al*., 2019). Accordingly, bacterial loads in the taproot-to-hypocotyl region were drastically reduced in H7996 compared to Marmande, confirming the remarkable bacterial restriction ability of this cultivar (Fig. S1b and (Planas-Marquès *et al*., 2019)).

To identify defense-associated anatomical and physico-chemical modifications in H7996 after infection with *R. solanacearum* compared to Marmande we performed histochemical, spectroscopic and gene expression analysis. For this, plants were infected with a 10^7 *R. solanacearum* solution or mock through their roots using the soil-drench method and then we collected tissue containing 10^5 CFU g^{-1} tissue of bacteria at the taproot-to-hypocotyl transition area, located approximately 1 cm below ground (Fig. S1a). Marmande reached 10^5 CFU g^{-1} tissue at around 4 dpi, while the resistant H7996 took approximately 9 days to do so (Fig. S2). We have previously observed that the root-to-hypocotyl area constitutes a key bottleneck for bacterial progression inside the plant (Zuluaga et al., 2015; Puigvert et al., 2017; Planas-Marquès et al., 2019), being thus an ideal target zone for analysis of structural defense responses.

We first analyzed ultraviolet (UV) autofluorescence of transverse cross-sections of the taproot-to-hypocotyl region, indicative of phenolic compounds (Donaldson, 2020). To focus on cell wall-deposited phenolic compounds, soluble phenolic compounds were removed with ethanol prior to observation as reported (Pouzoulet *et al*., 2013; Araujo *et al*., 2014). Infection with *R. solanacearum* induced a strong UV signal emitted from the walls of the vessels, and also from surrounding xylem parenchyma cells and tracheids in resistant H7996 (Figs. 1b, c). This enhanced autofluorescence was not observed in the susceptible

variety Marmande nor in mock-treated samples (Fig. 1b, c). In tissues outside the vascular area, inoculation resulted in a decrease of autofluorescence in both susceptible and resistant tomato lines.

Spectroscopic analysis reveals *R. solanacearum*-induced deposition of suberin and accumulation of tyramine-derived amides in resistant H7996 tomato and lignin structural modifications in susceptible Marmande tomato

In order to decipher the composition of the cell wall-deposited compounds we used nuclear magnetic resonance (2D-HSQ NMR), one of the most powerful tools for plant cell wall structural analysis providing information on the composition and linkages in lignin/suberin polymers (Ralph and Landucci, 2010; Correia *et al*., 2020). 2D-HSQC spectra of infected or mock-treated taproot-to-hypocotyl transition zones of H7996 and Marmande tomato plants were obtained and the main lignin and suberin substructures identified are shown in Fig. 2, while the chemical shifts of the assigned cross-signals are detailed in Table S2. Importantly, the aliphatic region of the 2D-HSQC spectra revealed that H7996 infected plants were more enriched in poly-aliphatic structures characteristic of suberin (magenta-colored signals), compared to its mock control (Fig 2a). Related to this, an olefinic cross-signal of unsaturated fatty acid structures (UF, δ_C/δ_H 129.4/5.31), typical of suberin, was also found to be increased in the HSQC spectrum of the infected H7996 tomato. A rough estimate based on the integration of lignin and suberin HSQC signals, revealed that the suberin/lignin ratio in *R. solanacearum*-infected H7996 plants was doubled compared to mock-treated plants, evidencing an increase in suberin deposition as a consequence of the bacterial infection. Interestingly, signals compatible with feruloylamides (FAm_7; δ_C/δ_H 138.6/7.31) and with tyramine-derived amides (Ty in orange; δ_C/δ_H 129.3/6.92, 114.8/6.64, 40.5/3.29 and 34.2/2.62) were exclusively found in the spectrum of infected H7996 plants, suggesting the presence of feruloyltyramine exclusively in these samples (Fig. 2a). Since tyramines have been found as structural components co-ocurring with suberin (Bernards *et al*., 1995; Bernards and Lewis, 1998), which generates physically and chemically resistant barriers (He and Ding, 2020), our results substantiate the hypothesis of suberin as an important defense element against *R. solanacearum* infection in resistant tomato plants. On

the contrary, the 2D-HSQC spectra from the Marmande variety did not display notable variations between mock and infected plants in the signals corresponding to suberin, tyramine-related structures nor feruloylamides (Fig 2a).

Interestingly, 2D-HSQC NMR spectra also revealed significant structural modifications in the composition of lignin and the distribution of linkages in tomato plants after infection. Lignins with lower S/G ratios are more branched (condensed) and recalcitrant towards pathogen attack (Iiyama *et al*., 2020). Therefore, lignin in inoculated H7996, with an S/G ratio of 1.0 should be, a priori, more resistant than the lignin in inoculated Marmande plants (S/G ratio of 1.5). 2D-HSQC analysis revealed that the infection of susceptible Marmande plants resulted in an increase of the S/G ratio and a clear reduction of all major lignin linkages (β–*O*–4′, β–5′ and β–β′; reduction in roughly 9%, 43% and 46%, respectively), evidencing that a lignin depolymerization process took place (Fig. 2a). In contrast, infected H7996 tomato displayed a slight decrease of the S/G ratio, and only β–*O*–4′ linkages (the easiest to degrade in the lignin polymer) were significantly reduced, while the β–5′ and β–β′ were not so affected as in the case of Marmande plants. In this context, the major reduction in lignin linkages observed in Marmande after infection could explain, at least in part, its higher susceptibility to the pathogen.

Histochemical analysis reveals the formation of structural vascular coatings containing suberin and ferulate/feruloylamide in resistant H7996 tomato in response to *R. solanacearum* infection

To confirm our spectroscopic data, we histochemically analyzed taproot-to-hypocotyl transition zone samples of mock and infected H7996 and Marmande tomato plants. Observation of Phloroglucinol-HCl stained sections under brightfield microscopy (Wiesner staining) (Pomar *et al*., 2002; Pradhan Mitra and Loqué, 2014), showed that mock and infected H9776 (resistant) as well as mock Marmande (susceptible) samples showed a red-purple color characteristic of the reaction of phloroglucinol-HCl in vessels and fibers, indicative of lignin (Fig. 3a). In contrast, infected Marmande sections exhibited reduced phloroglucinol-HCl staining, suggesting a change in composition of xylem lignin upon

337 infection (Fig. 3a). This observation is in agreement with the structural changes specifically
338 detected in the lignin structure of infected Marmande plants by 2D-HSQC NMR (Fig. 2a),
339 which suggest lignin depolymerization and may partly underscore the high susceptibility of
340 this tomato variety.
341
342 UV illumination of phloroglucinol-HCl-stained samples allows quenching the
343 autofluorescence from lignin and hence detect residual cell wall autofluorescence, which
344 has been associated with suberin deposits (Baayen and Elgersma, 1985; Rioux *et al*., 1998;
345 Pouzoulet *et al*., 2013). Under these conditions, the increased autofluorescence observed in
346 the vascular coating regions of infected H7996 tomato plants was not quenched in
347 phloroglucinol-HCl stained samples (Fig. 3a, b). A more detailed observation revealed that
348 this non-quenched autofluorescence was localized in specific regions compatible with (i)
349 intervessel and vessel-parenchyma pit membranes or pit chamber walls and (ii) parenchyma
350 coatings with fluorescent signals enriched in intracellular spaces (Fig 3c).
351
352 Next, we analyzed whether the pathogen-induced coating of vessels observed in H7996
353 correlated also with an increase in ferulates, a major suberin component. We performed
354 KOH treatment of plant tissues, which specifically shifts the UV fluorescence of
355 ferulate/feruloylamide to green, allowing its detection (Carnachan and Harris, 2000; Harris
356 and Trethewey, 2010; Donaldson and Williams, 2018). UV autofluorescence of vascular
357 coatings in response to *R. solanacearum* infection in resistant H7996 shifted from blue to a
358 strong green color upon treatment with alkali (1N KOH) (Fig. S3a). This indicated that the
359 *R. solanacearum*-induced xylem vasculature feruloylation was specific to resistant H7996,
360 as the fainter blue autofluorescence observed in mock-treated resistant H7996 or
361 susceptible Marmande tissues did not change to green at high pH in either early (Fig. S3a,
362 b) or late (Fig. S3c) stages of infection.
363
364 To corroborate that the ferulate/feruloylamide accumulation in infected H7996 tomato was
365 related with vascular suberization, we combined the ferulate-specific UV-alkali treatment
366 described above with Sudan IV staining, which binds aliphatic components of suberin to
367 produce a reddish-brown coloration. This revealed suberization in the taproot-to-hypocotyl

area of *R. solanacearum*-infected H7996 plants, xylem vessel walls as well as the layers of vessels, parenchyma cells and tracheids in the immediate vicinity (Fig. 4). In the periphery of suberized cells, a green signal from UV-alkali was observed (Fig. 4), which may indicate ferulate/feruloylamide deposition indicative of a preceding stage towards suberization in this cell layer. In comparison, no positive Sudan IV or UV-alkali staining was detected in infected Marmande or mock-treated tomato plants. Together, suberized and feruloylated layers of parenchyma cells, vessels and tracheids might form a "suberization zone" creating a strong physico-chemical barrier to limit *R. solanacearum* spread from the colonized xylem vessel lumen.

R. solanacearum infection activates the biosynthesis of aliphatic suberin precursors and feruloylamide, and aliphatic esterification of ferulic acid in the vasculature of resistant H7996

Since a differential accumulation of suberin-compatible compounds was specifically observed in infected H7996, we surmised that genes related to suberin and feruloylamide synthesis, as well as ferulic acid esterification to aliphatics may be upregulated in resistant tomato in response to *R. solanacearum* invasion. To test this hypothesis, we analyzed: i) expression of genes in the phenylpropanoid and suberin biosynthesis pathways, which provide the necessary precursors for the ligno-suberin heteropolymer; ii) the feruloyl transferase FHT (ASFT/HHT in Arabidopsis), which is involved in the formation of ferulate esters of fatty acyl compounds necessary to form suberin and soluble waxes (Molina *et al*., 2009; Gou *et al*., 2009; Serra *et al*., 2010); and iii) N-hydroxycinnamoyl transferases (*THT*), which are involved in the synthesis of HCAAs such as feruloyltyramine, which is found on the lignin-like polymer and in the soluble phenolic fraction of some suberized tissues (Negrel *et al*., 1993; Schmidt *et al*., 1999) .

Quantitative RT-PCR from xylem vascular tissue obtained from the taproot-to-hypocotyl zone in *R. solanacearum*- or mock-treated H7996 and Marmande plants showed specific upregulation of all genes analyzed from the suberin biosynthetic pathway in H7996 infected plants compared to the mock controls (Fig. 5, S4). These included essential suberin

biosynthesis genes such as *CYP86A1* and *CYP86B1* (fatty acid oxidation), *FAR* (primary alcohol generation), *KCSs* (fatty acid elongases) and *GPAT5* (acylglycerol formation). In addition, feruloyl transferase *FHT* (*ASFT/HHT* in Arabidopsis), was also strongly upregulated in infected H7996 plants (Fig. 5 and S5b). Regarding *THT*, in tomato we identified five putative homologs (Fig S6a), all induced by infection in the vascular tissue of H7996 (Fig. 5 and S6b). Among them, *SlTHT1-3* showed the strongest upregulation in H7996 after infection (Fig. 5 and S6b). In comparison, *R. solanacearum* infection had only a modest effect on genes related to phenylpropanoid pathway as only upregulation was detected in the first enzyme of the pathway (PAL) (Fig. 5 and S7).

Together, these data indicate that upregulation of genes involved in the formation of aliphatic suberin precursors, ferulic acid esterification to aliphatics (FHT) and production of HCAAs, such as feruloyltyramine (THT), constitute a very specific response of H7996 plants that takes place in the vasculature upon *R. solanacearum* infection. Further, these data are in agreement with NMR data of infected H7996, which showed a specific increase in insoluble fatty acid structures typical of suberin as well as the appearance of signals from structural tyramine-derived amides and feruloylamides (Fig. 2a).

Overexpression of *SlTHT1-3* in a susceptible tomato cultivar confers resistance to R. *solanacearum*

Based on our results, we set to determine whether overexpressing genes involved in ferulic acid esterification to suberin aliphatics and feruloylamide biosynthesis, such as *SlFHT* and *SlTHT1-3*, respectively, would increase resistance against *R. solanacearum* in a susceptible tomato background. First, we obtained transgenic tomato lines stably overexpressing *SlFHT* on a susceptible Marmande background (Fig. S8). Under normal growth conditions these lines are morphologically undistinguishable from wild-type, although they display a subtle increase in fresh weight (Fig. S9). We analyzed symptom progression and bacterial colonization. *SlFHT* overexpression lines showed a slight delay in disease progression (Fig. 6a) and moderately milder symptoms. The taproot-to-hypocotyl of *SlFHT* overexpressors

displayed a slight reduction in bacterial loads after soil-soak inoculation in comparison to Wt tomato (Fig. 6b).

Regarding *SlTHT1-3*, the corresponding tomato overexpressing line was readily available on a Moneymaker background (Campos *et al*., 2014). This line has been shown to overaccumulate soluble HCAA such as feruloyltyramine and also the hormone salicylic acid (SA) upon infection with *Pseudomonas syringae* pv. tomato (Campos *et al*., 2014). It is worth noting that tomato plants overexpressing *SlTHT1-3* display a slight decrease in fresh weight compared to wild-type plants, although with the naked eye they appear undistinguishable (Fig. S10). As expected, the Moneymaker tomato cultivar showed similar susceptibility to *R. solanacearum* as Marmande (Fig. 7a, b). In contrast, overexpression of *SlTHT1-3* resulted in a dramatic increase of resistance against *R. solanacearum,* with disease progressing remarkably slower in this line compared to wild type (Fig. 7a, b). Importantly, bacterial loads were significantly lower in the taproot-to-hypocotyl and hypocotyl of the *SlTHT1-3* overexpressor after soil inoculation in comparison to Wt tomato (Fig. 7c). Similarly, direct leaf inoculation also showed severe bacterial growth restriction in the *THT1-3* overexpressing line (Fig. S11a). Further, we monitored the colonization patterns of a *R. solanacearum* GFP reporter strain after stem inoculation of the *SlTHT1-3* overexpressing line compared to Wt. In transverse stem cross-sections of 6 dpi plants, bacteria stayed confined near the inoculation point in the *35S::SlTHT1-3* line whereas they spread unrestrictedly in susceptible wild type stems from the inoculation point and at least 3 cm up and downwards (Fig. 7d, e and S11b).

Concomitant with the observed restriction of *R. solanacearum* colonization, an increase in autofluorescence around the vasculature was observed in the *SlTHT1-3* overexpressor (Fig. 8a). At similar bacterial loads, Wt did not display such enhanced vascular fluorescence. Phloroglucinol-HCl staining did not quench the paravascular autofluorescence in *SlTHT1-3* (Fig. 8a, d), indicating that similar to what was previously observed for H7996, the observed increase in wall-bound phenolic deposits did not only correspond to lignin. To gain a deeper insight into the composition of the *R. solanacearum*-induced vascular deposits in *SlTHT1-3* overexpressing plants we performed combined Sudan IV-alkali

staining (Fig. 8b, c, e). Treatment with alkali resulted in a clear blue-to-green shift of UV autofluorescence around xylem vessels occurring specifically in the *SlTHT1-3* overexpressor upon infection, which reveals the presence of ferulates/feruloylamides as part of the observed vascular deposits. In contrast, no positive Sudan IV staining was detected, indicating that a canonical suberin polyester does not seem to be part of vascular coatings in *SlTHT1-3* overexpressing plants. Since Sudan IV only stains specific moieties of the complex suberin heteropolymer, we cannot rule out that the observed vascular deposits in *SlTHT1-3* are formed by a non-canonical ligno-suberin heteropolymer that does not react with Sudan IV. Further investigation will be needed in order to ascertain the exact nature of the *R. solanacearum*-induced vascular deposits in the *SlTHT1-3* overexpressor. In conclusion, our data clearly show that *StTHT1-3* ectopic expression provides a very effective resistance mechanism against *R. solanacearum* -potentially mediated by accumulation of elevated amounts of HCAAs such as feruloyltyramine-, which drastically restricts vascular colonization, preventing bacterial spread and blocking the onset of disease.

Discussion

Ligno-suberin deposits in vascular cell walls and feruloyltyramine accumulation acts as a resistance mechanism restricting *R. solanacearum* colonization in resistant tomato

In our study, resistant tomato (H7996) was observed to react aggressively to *R. solanacearum* infection by reinforcing the walls of vessels and the surrounding parenchyma cells with UV autofluorescent phenolic deposits (Fig. 1). An increase in autofluorescence had been previously reported in another resistant tomato variety, LS-89, although its composition was not precisely defined (Ishihara *et al*., 2012). Histochemical analysis of vascular coatings in resistant tomato upon *R. solanacearum* infection showed that suberin-associated autofluorescence was prominent in the vasculature, in line with previous reports using TEM that showed thickening of the pit membranes accumulating electron-dense material in tomato plants resistant to *R. solanacearum* (Nahako *et al*., 2000 and 2004). The suberin nature of these coatings was further supported by the positive Sudan IV staining of vessels and surrounding parenchyma cells of H7996 taproot-to-hypocotyl transition zone

upon infection (Fig. 4). These results are in agreement with coatings detected in tomato plants resistant to *Verticillium albo-atrum* (Robb *et al*., 1991), where suberin and lignin were both deposited in intercellular spaces between parenchyma cells adjoining a xylem vessel or infusing and occluding pit membranes coatings (Robb *et al*., 1991; Street *et al*., 1996). Besides, inhibition of the phenylpropanoid pathway inhibited the formation of both lignin and suberin coatings (Street *et al*., 1996), in agreement with the ferulic acid requirement to correctly deposit suberin (Andersen *et al*., 2021) and reinforcing our observations of the presence of a ferulate/feruloylamide-derived polymer detected in H7996 *R. solanacearum* (Fig. 4). In line with this, NMR data of resistant H7996 tomato vascular tissue revealed the presence of tyramine-derived amides and feruloylamides incorporated into the cell wall and also an enrichment in poly-aliphatic structures characteristic of suberin (Fig. 2) (Graça, 2015; Legay *et al*., 2016; Figueiredo *et al*., 2020).

Beyond histochemistry and spectroscopic signature detections, further evidence supporting the nature of these ligno-suberin coatings as responsible of the resistance observed in H7796 to *R. solanacearum* was unequivocally provided transcriptionally using gene markers. Tissues undergoing suberization have to go through a complex reprogramming involving a network of metabolic pathways, in order to produce the precursors of the polymer and their polymerization into the matrix (Lashbrooke *et al*., 2016). Transcriptional reprogramming associated to suberin biosynthesis was clearly observed in the taproot-to-hypocotyl transition zone vascular tissue of resistant H7996 tomato upon infection with *R. solanacearum* (Fig. 5). Interestingly, PAL, which showed modest upregulation in resistant H7996, had been previously defined as a rate-limiting enzyme of phenylpropanoid pathway (Faragher and Brohier, 1984; Howles *et al*., 1996). Considering this, the observed upregulation could provide more tyramine and feruloyl-CoA, which together with the upregulation of *THT* would be in agreement with the increased presence of feruloyltyramine detected by 2D-HSQC NMR (Figure 2a).

2D-HSQC NMR also revealed differences in the composition and structure of lignin between resistant and susceptible tomato cultivars after infection (Fig. 2). The amounts and the level of lignin of a particular tissue affect wall strength, degradability and pathogen

resistance (Cho et al., 2012; Mnich *et al*., 2020). However, its role in resistance/susceptibility responses is not fully understood. Part of the challenge lies in the fact that its composition seems to be less static than what was previously established. A large variety of lignin-like polymers may co-exist in plants depending on the developmental or environmental context. This becomes particularly relevant in plant-pathogen interactions, where a large variety of compounds linked to lignin differentially accumulate upon infection (Cho et al., 2012; Zeiss et al., 2019). The observed lignin structural differences after infection indicate that i) under basal conditions the two tomato varieties display differences in the composition and structure of lignin and ii) *R. solanacearum* infection affects very differently the lignin fraction in the two varieties: resistant tomato shows only a slight decrease in the S/G ratio that may be linked to an accumulation of the ligno-suberin heteropolymer, while susceptible Marmande undergoes pronounced depolymerization that correlates with a decrease in ferulate/feruloylamide (Fig. 3A). Although *R. solanacearum* has not been shown to be able to specifically depolymerize lignin, the pathogen secretes enzymes that can degrade cell wall polysaccharides and could participate in the observed Marmande stem collapse phenotype (Fig. 1A). In resistant H7996, on the other hand, vascular ligno-suberin-containing coatings would allow to create a hydrophobic barrier to prevent enzymes from accessing the cell wall substrates and at the same time create reinforcements, contributing to resistance to the pathogen. The fact that these reinforcements are rich in tyramine/feruloyltyramine, may further reinforce the structural barrier, providing rigidity and hampering cell wall digestibility by the pathogen's hydrolytic enzymes (Macoy *et al*., 2015; Zeiss *et al*., 2020). In addition to that, resistant H7996 may have evolved yet undiscovered mechanisms that directly prevent lignin degradation by the pathogen.

Overall, our data indicate that vascular coating with wall-bound ligno-suberized compounds may restrict horizontal spread of the bacterium (Fig 1). In comparison, susceptible tomato is either not able to induce such vascular coating upon *R. solanacearum* infection or induces a very weak response (Figs. 1, 3), potentially predisposing its vascular walls to disruption by the pathogen's cell wall degrading enzymes. Considering that both varieties seem to possess the metabolic components to build such barriers, the difference in

553 response may be a direct effect of the differential transcriptional activation of the pathway
554 in vascular tissue of H7996 compared to Marmande. The fact that varieties with moderate
555 resistance to *R. solanacearum* show intermediate restriction of colonization (Planas-
556 Marquès et al., 2019), indicate that the formation of these barriers may be a quantitative
557 trait. However, this also opens the possibility that the differential transcriptional activation
558 of the ligno-suberin pathway observed in resistant tomato may have evolved as an effective
559 mechanism to execute defense responses triggered by activation of an immune receptor
560 upon *R. solanacearum* recognition. Very few immune receptors involved in perception of
561 vascular wilt pathogens have been identified so far, and the mechanisms involved in
562 translating this recognition into effective defense responses in the vasculature remain vastly
563 unknown. Considering that the xylem is a dead tissue, it is expected that the surrounding
564 parenchyma cells will have a pivotal role in perception of the pathogen as well as the
565 signaling leading to the synthesis and wall-binding of the metabolites involved in vascular
566 coating structures, such as the one described here. In fact, xylem parenchyma cells have
567 been shown to synthesize vascular coating components in response to the wilt pathogen *V.*
568 *albo-atrum* (Street et al., 1986). However, how suberin is synthesized and deposited in the
569 xylem is still poorly defined. Exciting research currently ongoing in this area will certainly
570 help understanding the origin and transport of ligno-suberin components to form inducible
571 vascular deposits in response to pathogens. This will also help determining the exact point
572 of perception of the pathogen (at a cell type or tissular level). Identification of pathogen-
573 inducible pathways specifically occurring in resistant varieties such as the one presented
574 here open new avenues of research to shed light on this biologically and agronomically
575 relevant question.
576
577 Based on the above observations, we propose the following model (Fig. 9). When reaching
578 the xylem vessels of resistant H7996, *R. solanacearum* multiplies and tries to invade the
579 surrounding healthy vessels and parenchyma cells by degradation of the xylem pit
580 membranes and walls. Resistant tomato plants respond to *R. solanacearum* vascular
581 invasion depositing feruloyltyramine and other HCAA-tyramine derived compounds, and
582 suberin. These deposits would block the pit membrane access and serve as coatings of the
583 vessel walls and parenchyma cells present in the immediate vicinity of colonized vessels,

584 compartmentalizing the infection. These ligno-suberized layers together form a "zone of
585 ligno-suberization" creating a strong physico-chemical barrier to limit *R. solanacearum*
586 spread.
587
588 **Engineering tomato resistance against *R. solanacearum* by inducing the tyramine-**
589 **HCAA pathway**
590
591 Considering the observed accumulation of ligno-suberin and cell wall-linked
592 feruloyltyramine in resistant H7996 tomato in response to *R. solanacearum* infection, we
593 sought to understand the implications of overexpressing genes involved in the synthesis of
594 these compounds in susceptible tomato cultivars upon *R. solanacearum* infection. We
595 focused on *FHT* and *THT* and because their corresponding transcripts are upregulated in the
596 xylem vasculature of resistant tomato upon *R. solanacearum* infection (Fig. 5) and they are
597 the enzymes related with the synthesis of suberin ferulates and ether linked
598 feruloyltyramine, respectively.
599
600 *SlFHT* overexpression had a small effect on the responses of susceptible tomato against *R.*
601 *solanacearum*, showing a slight delay in wilting symptoms together with a slight decrease
602 of bacterial loads in the plant (Fig. 6). The fact that increasing the levels of FHT in
603 Marmande does only result in a marginal increase in resistance might be linked to a
604 shortfall of aliphatic precursors in this variety (Fig. 5), which constrain a subsequent
605 increase in suberin synthesis. In contrast, transgenic tomato overexpressing *SlTHT1-3* on a
606 susceptible background was highly resistant to *R. solanacearum* (Fig. 7). Importantly, this
607 transgenic line was previously shown to accumulate elevated amounts of soluble HCAAs
608 such as feruloyltyramine and also SA upon infection with the bacteria *Pseudomonas*
609 *syringae* pv. *tomato* (*Pto*) and to slightly but significantly restrict bacterial growth (Campos
610 *et al*., 2014). Since SA does not seem to play a major role in defense responses against *R.*
611 *solanacearum* (Hirsch et al., 2002; Hernández-Blanco et al., 2007; Hanemian et al., 2016),
612 accumulation of this hormone in *SlTHT1-3* overexpressing line may not be the major
613 underlying cause of the observed increase in resistance in this line. Alternatively, enhanced
614 production of tyramine-derived HCAAs may constitute an important defense strategy

against *R. solanacearum*. Feruloyltyramines exhibit antimicrobial activity (Fattorusso *et al.*, 1999; Novo *et al.*, 2017) and that they can be involved in plant priming or an adaptive strategy where plants are in a physiological state with improved defensive capacity (Zeiss *et al*., 2021). These tyramine-derived HCAAs overproduced in *SlTHT1-3* overexpressing plants may interfere with *R. solanacearum* colonization by becoming incorporated into the vascular and perivascular cell walls, providing a stronger cross-linking and restricting the movement of the pathogen inside the plant (Figure 8) but also partly by remaining soluble and acting as direct antimicrobial agents against the pathogen. *R. solanacearum* possesses a hydroxycinnamic acid degradation pathway and it has been shown that mutants that cannot degrade hydroxycinnamic acids are less virulent on tomato (Lowe-Power et al., 2015; Zhang *et al*., 2019), which clearly underscores the importance of HCAAs in the arms race taking place in this pathosystem. Considering that the ligno-suberin pathway and HCAAs are well-conserved across the plant kingdom (Philippe et al., 2020; Kashyap et al., 2021; Zeiss et al., 2021), these findings open the possibility to engineer disease resistance in other *R. solanacearum* hosts by manipulating these pathways. Interestingly, ligno-suberin deposits and accumulation of HCAAs have been reported in response to drought (Macoy et al., 2015; Zhang et al., 2020). Therefore, engineering these pathways could have a double impact both on biotic and abiotic stress responses, improving plant performance in the field under adverse conditions.

In conclusion, we have provided evidence of the formation of a "ligno-suberization zone" enriched in ether-linked feruloyltyramine and possibly related amides as an effective strategy to confine *R. solanacaerum* into infected vessels of resistant tomato plants, preventing horizontal spread of the pathogen into healthy tissues and delaying disease symptoms. Resistance against *R. solanacearum* can be attained in susceptible tomato background by stably overexpressing *THT*, potentially contributing In the future, it will be interesting to investigate the contribution of HCAAs and suberin to resistance against the pathogen, the mechanisms whereby *R. solanacearum* perception leads to the formation of a ligno-suberin coatings around the vasculature in resistant tomato varieties. Increasing the spatio-temporal resolution of the tomato-*R. solanacearum* interaction will be instrumental to reach a deeper insight into structural resistance mechanisms. Also, since vascular

confinement has been reported in different plant species as a means of resistance against various vascular wilt pathogens (De Ascensao and Dubery, 2000; Martín *et al*., 2008; Xu *et al*., 2011; Sabella *et al*., 2018), the level of conservation of vascular ligno-suberin deposition and HCAAs as a constituent of vascular coatings and part of a resistance mechanism remains to be determined.

Acknowledgements

The authors would like to thank Gabriel Castrillo and Nico Geldner for inspiring discussions. We also thank Marc Planas-Marquès for helpful comments and María Pilar López Gresa (IBMCP-UPV) for kindly sharing the tomato THT seeds. Research is funded by MCIN/AEI/10.13039/501100011033 (NSC, MV), MCIN/AEI/PID2019-110330GB-C21 (MF, OS), through the "Severo Ochoa Programme for Centres of Excellence in R&D" (SEV-2015-0533 and CEX2019-000902-S funded by MCIN/AEI/ 10.13039/501100011033). , and by the Spanish National Research Council (CISC) pie-201620E081 (JR, AG). AK is the recipient of a Netaji Subhas - Indian Council of Agricultural Research International Fellowship. This work was also supported by the CERCA Programme/Generalitat de Catalunya. We acknowledge support of the publication fee by the CSIC Open Access Publication Support Initiative through its Unit of Information Resources for Research (URICI).

Author Contribution

AK designed and performed experiments, interpreted data and wrote the manuscript.

ALJ-J performed the experiments required for the second submission of the manuscript.

WZ performed experiments.

MC performed experiments, interpreted data and reviewed the manuscript.

SS conducted preliminary spectroscopy experiments and reviewed the manuscript.

JR isolated the lignin/suberin fractions and conducted the 2D-HSQC NMR analysis, including data interpretation.

AG isolated the lignin/suberin fractions and conducted the 2D-HSQC NMR analysis, including data interpretation.

AL conducted preliminary spectroscopy experiments and reviewed the manuscript.

OS conducted histopathology staining experiments, interpreted data and reviewed the manuscript.

MF interpreted data and reviewed the manuscript.

MV designed experiments, interpreted data and reviewed the manuscript.

NSC conceptualized the research, designed experiments, interpreted data and wrote the manuscript.

Data Availability

The data that support the findings of this study are available from the corresponding author upon reasonable request.

References

Álvarez, B., Biosca, E.G., and López, M.M. (2010). On the life of *Ralstonia solanacearum*, a destructive bacterial plant pathogen. In Technology and education topics in applied microbiology and microbial biotechnology, A. Méndez-Vilas, ed (Badajoz: Formatex), pp. 267–279.

Andersen, T.G., Molina, D., Kilian, J., Franke, R.B., Ragni, L., and Geldner, N. (2021). Tissue-autonomous phenylpropanoid production is essential for establishment of root barriers. Curr. Biol. **31**: 965-977.

Araujo, L., Bispo, W.M.S., Cacique, I.S., Moreira, W.R., and Rodrigues, F.A. (2014). Resistance in mango against infection by *Ceratocystis fimbriata*. Phytopathology **104**: 820–833.

De Ascensao, A.R.D.C.F. and Dubery, I.A. (2000). Panama disease: cell wall reinforcement in banana roots in response to elicitors from *Fusarium oxysporum* f. sp. *cubense* race four. Phytopathology **90**: 1173–1180.

Baayen, R.P. and Elgersma, D.M. (1985). Colonization and histopathology of susceptible and resistant carnation cultivars infected with *Fusarium oxysporum* f. sp. *dianthi* . Netherlands J. Plant Pathol. **91**: 119–135.

Benhamou, N. (1995). Ultrastructural and cytochemical aspects of the response of eggplant parenchyma cells in direct contact with *Verticillium*-infected xylem vessels. Physiol.

Mol. Plant Pathol. **46**: 321–338.

Bernards, M., Lopez, M., Zajicek, J., and Lewis, N. (1995). Hydroxycinnamic acid-derived polymers constitute the polyaromatic domain of suberin. J. Biol. Chem. **270**: 7382–7386.

Bernards, M.A. (2002). Demystifying suberin. Can. J. Bot. **80**: 227–240.

Bernards, M.A. and Lewis, N.G. (1998). The macromolecular aromatic domain in suberized tissue: a changing paradigm. Phytochemistry **47**: 915–933.

Biggs, A. (1984). Intracellular suberin: occurrence and detection in tree bark. IAWA Bull. **5**: 243–248.

Caldwell, D., Kim, B., and Iyer-Pascuzzi, A.S. (2017). *Ralstonia solanacearum* differentially colonizes roots of resistant and susceptible tomato plants. Phytopathology **107**: 528–536.

Campos, L., Lisón, P., López-Gresa, M.P., Rodrigo, I., Zacarés, L., Conejero, V., and Bellés, J.M. (2014). Transgenic tomato plants overexpressing tyramine N -hydroxycinnamoyltransferase exhibit elevated hydroxycinnamic acid amide levels and enhanced resistance to *Pseudomonas syringae* . Mol. Plant-Microbe Interact. **27**: 1159–1169.

Carnachan, S.M. and Harris, P.J. (2000). Ferulic acid is bound to the primary cell walls of all gymnosperm families. Biochem. Syst. Ecol. **28**: 865–879.

Cho, K., Kim, Y., Wi, S.J., Seo, J.B., Kwon, J., Chung, J.H., Park, K.Y., and Nam, M.H. (2012). Nontargeted metabolite profiling in compatible pathogen-inoculated tobacco (*Nicotiana tabacum* L. cv. Wisconsin 38) using UPLC-Q-TOF/MS. J. Agric. Food Chem. **60**: 11015–11028.

Correia, V.G., Bento, A., Pais, J., Rodrigues, R., Haliński, P., Frydrych, M., Greenhalgh, A., Stepnowski, P., Vollrath, F., King, A.W.T. *et al.* (2020). The molecular structure and multifunctionality of the cryptic plant polymer suberin. Mater. Today Bio **5**: 100039.

Cruz, A.P.Z., Ferreira, V., Pianzzola, M.J., Siri, M.I., Coll, N.S., and Valls, M. (2014). A novel, sensitive method to evaluate potato germplasm for bacterial wilt resistance using a luminescent *Ralstonia solanacearum* reporter strain. Mol. Plant-Microbe Interact. **27**: 277–285.

Digonnet, C., Martinez, Y., Denancé, N., Chasseray, M., Dabos, P., Ranocha, P., Marco, Y., Jauneau, A., and Goffner, D. (2012). Deciphering the route of *Ralstonia solanacearum* colonization in *Arabidopsis thaliana* roots during a compatible interaction: Focus at the plant cell wall. Planta **236**: 1419–1431.

Donaldson, L. (2020). Autofluorescence in plants. Molecules **25**: 2393.

Donaldson, L. and Williams, N. (2018). Imaging and spectroscopy of natural fluorophores in pine needles. Plants **7**: 10.

Dorado, J., Almendros, G., Field, J.A., and Sierra-alvarez, R. (2001). Infrared spectroscopy analysis of hemp (*Cannabis sativa*) after selective delignification by *Bjerkandera* sp . at different nitrogen levels. Enzyme Microb. Technol. **28**: 550–559.

Falter, C., Ellinger, D., Von Hulsen, B., Heim, R., and Voigt, C.A. (2015). Simple preparation of plant epidermal tissue for laser microdissection and downstream quantitative proteome and carbohydrate analysis. Front. Plant Sci. **6**: 194.

Faragher, J.D. and Brohier, R.L. (1984). Anthocyanin accumulation in apple skin during ripening: regulation by ethylene and phenylalanine ammonia-lyase. Sci. Hortic. **22**: 89–96.

Fattorusso, E., Lanzotti, V., and Taglialatela-Scafati, O. (1999). Antifungal N-feruloylamides from roots of two *Allium* species. Plant Biosyst. **133**: 199–203.

Figueiredo, R., Portilla Llerena, J.P., Kiyota, E., Ferreira, S.S., Cardeli, B.R., de Souza, S.C.R., dos Santos Brito, M., Sodek, L., Cesarino, I., and Mazzafera, P. (2020). The sugarcane ShMYB78 transcription factor activates suberin biosynthesis in *Nicotiana benthamiana*. Plant Mol. Biol. **104**: 411–427.

Gleave, A.P. (1992). A versatile binary vector system with a T-DNA organisational structure conducive to efficient integration of cloned DNA into the plant genome. Plant Mol. Biol. **20**: 1203–1207.

Gou, J.-Y., Yu, X.-H., and Liu, C.-J. (2009). A hydroxycinnamoyltransferase responsible for synthesizing suberin aromatics in Arabidopsis. Proc. Natl. Acad. Sci. **106**: 18855–18860.

Graça, J. (2010). Hydroxycinnamates in suberin formation. Phytochem. Rev. **9**: 85–91.

Graça, J. (2015). Suberin: the biopolyester at the frontier of plants. Front. Chem. **3**: 62.

Grimault, V., Anais, G., and Prior, P. (1994). Distribution of *Pseudomonas*

solanacearum in the stem tissues of tomato plants with different levels of resistance to bacterial wilt. Plant Pathol. **43**: 663–668.

Hanemian, M. et al. (2016). Arabidopsis CLAVATA1 and CLAVATA2 receptors contribute to *Ralstonia solanacearum* pathogenicity through a miR169-dependent pathway. New Phytol. **211**: 502–515.

Hao, Z. *et al.* (2014). Loss of arabidopsis GAUT12/IRX8 causes anther indehiscence and leads to reduced G lignin associated with altered matrix polysaccharide deposition. Front. Plant Sci. **5**: 357.

Harris, P.J. and Trethewey, J.A.K. (2010). The distribution of ester-linked ferulic acid in the cell walls of angiosperms. Phytochem. Rev. **9**: 19–33.

He, M. and Ding, N. (2020). Plant unsaturated fatty acids : multiple roles in stress response. Front. Plant Sci. **11**: 562785.

Hernández-Blanco, C. et al. (2007). Impairment of cellulose synthases required for Arabidopsis secondary cell wall formation enhances disease resistance. Plant Cell **19**: 890–903.

Hirsch, J., Deslandes, L., Feng, D.X., Balagué, C., and Marco, Y. (2002). Delayed symptom development in ein2-1, an Arabidopsis ethylene-insensitive mutant, in response to bacterial wilt caused by Ralstonia solanacearum. Phytopathology **92**: 1142–1148.

Howles, P.A., Sewalt, V.J.H., Paiva, N.L., Elkind, Y., Bate, N.J., Lamb, C., and Dixon, R.A. (1996). Overexpression of L-phenylalanine ammonia-lyase in transgenic tobacco plants reveals control points for flux into phenylpropanoid biosynthesis. Plant Physiol. **112**: 1617–1624.

Iiyama, K., Lam, T.B.T., and Stone, B. (2020). Covalent cross-links in the cell wall. Plant Physiol. **104**: 315–320.

Ishihara, T., Mitsuhara, I., Takahashi, H., and Nakaho, K. (2012). Transcriptome analysis of quantitative resistance-specific response upon *Ralstonia solanacearum* infection in tomato. PLoS One **7(10):** e46763.

Jhu, M., Farhi, M., Wang, L., Philbrook, R.N., Belcher, M.S., Nakayama, H., Zumstein, K.S., Rowland, S.D., Ron, M., Shih, P.M., *et al.* (2021). Lignin-based resistance to *Cuscuta campestris* parasitism in Heinz resistant tomato cultivars.

bioRxiv. https://doi.org/10.1101/706861.

Jones, J.D.G. and Dangl, J.L. (2006). The plant immune system. Nature **444**: 323–329.

Joo, Y., Kim, H., Kang, M., Lee, G., Choung, S., Kaur, H., Oh, S., Choi, J.W., Ralph, J., Baldwin, I.T., *et al.* (2021). Pith-specific lignification in *Nicotiana attenuata* as a defense against a stem-boring herbivore. New Phytol. **232**: 332–344.

Kashyap, A., Planas-marquès, M., Capellades, M., Valls, M, and Coll, N.S. (2021). Blocking intruders : inducible physico-chemical barriers against plant vascular wilt pathogens. J. Exp. Bot. **72**: 184–198.

Kim, S.G., Hur, O.S., Ro, N.Y., Ko, H.C., Rhee, J.H., Sung, J.S., Ryu, K.Y., Lee, S.Y., and Baek, H.J. (2016). Evaluation of resistance to *Ralstonia solanacearum* in tomato genetic resources at seedling stage. Plant Pathol. J. **32**: 58–64.

Kutscha, N.P. and Gray, J.R. (1972). The suitability of certain stains for studying lignification in balsam fir, Abies balsamina (L.) Mill. Tech. Bull. 53: 1–51.

Lahlali, R., Song, T., Chu, M., Yu, F., Kumar, S., Karunakaran, C., and Peng, G. (2017). Evaluating changes in cell-wall components associated with clubroot resistance using fourier transform infrared spectroscopy and RT-PCR. International J. Mol. Sci. **18**: 2058.

Lashbrooke, J., Cohen, H., Levy-Samocha, D., Tzfadia, O., Panizel, I., Zeisler, V., Massalha, H., Stern, A., Trainotti, L., Schreiber, L., *et al.* (2016). MYB107 and MYB9 homologs regulate suberin deposition in angiosperms. Plant Cell **28**: 2097–2116.

Legay, S., Guerriero, G., André, C., Guignard, C., Cocco, E., Charton, S., Boutry, M., Rowland, O., and Hausman, J.F. (2016). MdMyb93 is a regulator of suberin deposition in russeted apple fruit skins. New Phytol. **212**: 977–991.

Liu, H., Zhang, S., Schell, M.A., and Denny, T.P. (2005). Pyramiding unmarked deletions in *Ralstonia solanacearum* shows that secreted proteins in addition to plant cell-wall-degrading enzymes contribute to virulence. Mol. Plant-Microbe Interact. **18**: 1296–1305.

Lopes, M. H., Neto, C. P., Barros, A. S., Rutledge, D., Delgadillo, I., and Gil, A. M. (2000). Quantitation of aliphatic suberin in *Quercus suber* L. cork by FTIR spectroscopy and solid-state 13C-NMR spectroscopy. Biopolymers **57**: 344-351.

Lowe-Power, T.M., Ailloud, F., and Allen, C. (2015). Hydroxycinnamic Acid Degradation, a Broadly Conserved Trait, Protects *Ralstonia solanacearum* from Chemical Plant Defenses and Contributes to Root Colonization and Virulence. Mol. Plant-Microbe Interact. **28**: 286–297.

Lowe-Power, T.M., Khokhani, D., and Allen, C. (2018). How *Ralstonia solanacearum* exploits and thrives in the flowing plant xylem environment. Trends Microbiol. **26**: 929–942.

Lulai, E.C. and Corsini, D.L. (1998). Differential deposition of suberin phenolic and aliphatic domains and their roles in resistance to infection during potato tuber (*Solanum tuberosum* L.) wound-healing. Physiol. Mol. Plant Pathol. **53**: 209–222.

Macoy, D.M., Kim, W.Y., Lee, S.Y., and Kim, M.G. (2015). Biosynthesis, physiology, and functions of hydroxycinnamic acid amides in plants. Plant Biotechnol. Rep. **9**: 269–278.

Macoy, D.M., Kim, W.Y., Lee, S.Y., and Kim, M.G. (2015). Biotic stress related functions of hydroxycinnamic acid amide in plants. J. Plant Biol. **58**: 156–163.

Mahmoud, A.B., Danton, O., Kaiser, M., Han, S., Moreno, A., Algaffar, S.A., Khalid, S., Oh, W.K., Hamburger, M., and Mäser, P. (2020). Lignans, amides, and saponins from *Haplophyllum tuberculatum* and their antiprotozoal activity. Molecules **25**: 2825.

Mangin, B., Thoquet, P., Olivier, J., and Grimsley, N.H. (1999). Temporal and multiple quantitative trait loci analyses of resistance to bacterial wilt in tomato permit the resolution of linked loci. Genetics **151**: 1165–1172.

Martín, J.A., Solla, A., Coimbra, M.A., and Gil, L. (2005). Metabolic distinction of *Ulmus minor* xylem tissues after inoculation with *Ophiostoma novo-ulmi*. Phytochemistry **66**: 2458–2467.

Martín, J.A., Solla, A., Domingues, M.R., Coimbra, M.A., and Gil, L. (2008). Exogenous phenol increase resistance of *Ulmus minor* to dutch elm disease through formation of suberin-like compounds on xylem tissues. Environ. Exp. Bot. **64**: 97–104.

Mazier, M., Flamain, F., Nicolaï, M., Sarnette, V., and Caranta, C. (2011). Knock-down of both eIF4E1 and eIF4E2 genes confers broad-spectrum resistance against potyviruses in tomato. PLoS One **6(12):** e29595**.**

McGarvey, J.A., Denny, T.P., and Schell, M.A. (1999). Spatial-temporal and quantitative analysis of growth and EPS I production by *Ralstonia solanacearum* in resistant and susceptible tomato cultivars. Phytopathology **89**: 1233–1239.

Mnich, E. *et al.* (2020). Phenolic cross-links: building and de-constructing the plant cell wall. Nat. Prod. Rep. **37**: 919-961.

Molina, I., Li-Beisson, Y., Beisson, F., Ohlrogge, J.B., and Pollard, M. (2009). Identification of an Arabidopsis feruloyl-coenzyme a transferase required for suberin synthesis. Plant Physiol. **151**: 1317–1328.

Nakaho, K., Hibino, H., and Miyagawa, H. (2000). Possible mechanisms limiting movement of *Ralstonia solanacearum* in resistant tomato tissues. J. Phytopathol. **148**: 181–190.

Nakaho, K., Inoue, H., Takayama, T., and Miyagawa, H. (2004). Distribution and multiplication of *Ralstonia solanacearum* in tomato plants with resistance derived from different origins. J. Gen. Plant Pathol. 70:115–119.

Negrel, J., Javelle, F., and Paynot, M. (1993). Wound-induced tyramine hydroxycinnamoyl transferase in Potato (*Solanum tuberosum*) tuber discs. J. Plant Physiol. **142**: 518–524.

Negrel, J., Pollet, B., and Lapierre, C. (1996). Ether-linked ferulic acid amides in natural and wound periderms of potato tuber. Phytochemistry **43**: 1195–1199.

Novaes, E., Kirst, M., Chiang, V., Winter-sederoff, H., and Sederoff, R. (2010). Lignin and biomass: A negative correlation for wood formation and lignin content in trees. Plant Physiol. **154**: 555–561.

Novo, M., Silvar, C., Merino, F., Martínez-Cortés, T., Lu, F., Ralph, J., and Pomar, F. (2017). Deciphering the role of the phenylpropanoid metabolism in the tolerance of *Capsicum annuum* L. to *Verticillium dahliae* Kleb. Plant Sci. **258**: 12–20.

Pérez-Donoso, A.G., Sun, Q., Caroline Roper, M., Carl Greve, L., Kirkpatrick, B., and Labavitch, J.M. (2010). Cell wall-degrading enzymes enlarge the pore size of intervessel pit membranes in healthy and *Xylella fastidiosa*-infected grapevines. Plant Physiol. **152**: 1748–1759.

Planas-Marquès, M., Bernardo-Faura, M., Paulus, J., Kaschani, F., Kaiser, M., Valls, M., Van Der Hoorn, R.A.L., and Coll, N.S. (2018). Protease activities triggered by

Ralstonia solanacearum infection in susceptible and tolerant tomato lines. Mol. Cell. Proteomics **17**: 1112–1125.

Planas-Marquès, M., Kressin, J.P., Kashyap, A., Panthee, D.R., Louws, F.J., Coll, N.S., and Valls, M. (2019). Four bottlenecks restrict colonization and invasion by the pathogen *Ralstonia solanacearum* in resistant tomato. J. Exp. Bot. **71**: 2157–2171.

Philippe, G., Sørensen, I., Jiao, C., Sun, X., Fei, Z., Domozych, D.S., and Rose, J.K. (2020). Cutin and suberin: assembly and origins of specialized lipidic cell wall scaffolds. Curr. Opin. Plant Biol. **55**: 11–20.

Pomar, F., Merino, F., and Barceló, A.R. (2002). O-4-linked coniferyl and sinapyl aldehydes in lignifying cell walls are the main targets of the Wiesner (phloroglucinol-HCl) reaction. Protoplasma **220**: 17–28.

Pomar, F., Novo, M., Bernal, M.A., Merino, F., Barceló, A.R., and Barceló, A.R. (2004). Changes in stem lignins (monomer composition and crosslinking) and peroxidase are related with the maintenance of leaf photosynthetic integrity during *Verticillium* wilt in *Capsicum annuum*. New Phytol. **163**: 111–123.

Potter, C., Harwood, T., Knight, J., and Tomlinson, I. (2011). Learning from history, predicting the future: The UK dutch elm disease outbreak in relation to contemporary tree disease threats. Philos. Trans. R. Soc. B Biol. Sci. **366**: 1966–1974.

Pouzoulet, J., Jacques, A., Besson, X., Dayde, J., and Mailhac, N. (2013). Histopathological study of response of *Vitis vinifera* cv. Cabernet Sauvignon to bark and wood injury with and without inoculation by *Phaeomoniella chlamydospora*. Phytopathol. Mediterr. **52**: 313–323.

Pradhan Mitra, P. and Loqué, D. (2014). Histochemical staining of *Arabidopsis thaliana* secondary cell wall elements. J. Vis. Exp.: 87: e51381.

Puigvert, M., Guarischi-Sousa, R., Zuluaga, P., Coll, N.S., Macho, A.P., Setubal, J.C., and Valls, M. (2017). Transcriptomes of *Ralstonia solanacearum* during root colonization of *Solanum commersonii*. Front. Plant Sci. **8**: 370.

Ralph, J. and Landucci, L. (2010). NMR of lignins. In Heitner JA, Dimmel C, Scmidt DR eds. Lignin and Lignans: Advances in chemistry. Boca Raton, FL, USA: CRC Press, Taylor & Francis, 137–243.**Razem, F.A. and Bernards, M.A.** (2002). Hydrogen peroxide is required for poly(phenolic) domain formation during wound-induced

suberization. J. Agric. Food Chem. **50**: 1009–1015.

Rencoret, J., Kim, H., Evaristo, A.B., Gutiérrez, A., Ralph, J., and Del Río, J.C. (2018). Variability in lignin composition and structure in cell walls of different parts of macaúba (*Acrocomia aculeata*) Palm Fruit. J. Agric. Food Chem. **66**: 138–153.

Rico, A., Rencoret, J., Del Río, J.C., Martínez, A.T., and Gutiérrez, A. (2014). Pretreatment with laccase and a phenolic mediator degrades lignin and enhances saccharification of *Eucalyptus* feedstock. Biotechnol. Biofuels **7**: 6.

del Río, J.C., Rencoret, J., Gutiérrez, A., Kim, H., and Ralph, J. (2018). Structural characterization of lignin from Maize (*Zea mays* L.) fibers: evidence for diferuloylputrescine incorporated into the lignin polymer in Maize kernels. J. Agric. Food Chem. **66**: 4402–4413.

Rioux, D., Blais, M., Nadeau-Thibodeau, N., Lagacé, M., Des Rochers, P., Klimaszewska, K., and Bernier, L. (2018). First extensive microscopic study of butternut defense mechanisms following inoculation with the canker pathogen *Ophiognomonia clavigignenti-juglandacearum* reveals compartmentalization of tissue damage. Phytopathology **108**: 1237–1252.

Rioux, D., Nicole, M., Simard, M., and Ouellette, G.B. (1998). Immunocytochemical evidence that secretion of pectin occurs during gel (gum) and tylosis formation in trees. Phytopathology **88**: 494–505.

Rittinger, P.A., Biggs, A.R., and Peirson, D.R. (1986). Histochemistry of lignin and suberin deposition in boundary layers formed after wounding in various plant species and organs. Can. J. Bot. **65**: 1886–1892.

Robb, J., Lee, S.W., Mohan, R., and Kolattukudy, P.E. (1991). Chemical characterization of stress-induced vascular coating in tomato. Plant Physiol. **97**: 528–536.

Sabella, E., Luvisi, A., Aprile, A., Negro, C., Vergine, M., Nicolì, F., Miceli, A., and De Bellis, L. (2018). *Xylella fastidiosa* induces differential expression of lignification related-genes and lignin accumulation in tolerant olive trees cv. Leccino. J. Plant Physiol. **220**: 60–68.

Salas-González, I., Reyt, G., Flis, P., Custódio, V., Gopaulchan, D., Bakhoum, N., Dew, T.P., Suresh, K., Franke, R.B., Dangl, J.L., *et al.* (2021). Coordination

between microbiota and root endodermis supports plant mineral nutrient homeostasis. Science. **371**: eabd0695.

Schmidt, A., Grimm, R., Schmidt, J., Scheel, D., and Strackt, D. (1999). Cloning and expression of a potato cDNA encoding hydroxycinnamoyl- CoA:tyramine N-(hydroxycinnamoyl)transferase. J. Biol. Chem. **274**: 4273–4280.

Scortichini, M. (2020). The multi-millennial olive agroecosystem of salento (Apulia, Italy) threatened by *Xylella fastidiosa* subsp. Pauca: A working possibility of restoration. Sustain. **12**: 6700.

Serra, O., Figueras, M., Franke, R., Prat, S., and Molinas, M. (2010). Unraveling ferulate role in suberin and periderm biology by reverse genetics. Plant Signal. Behav. **5**: 953–958.

Serrano, M., Coluccia, F., Torres, M., L'Haridon, F., and Métraux, J.P. (2014). The cuticle and plant defense to pathogens. Front. Plant Sci. **5**: 274.

Smith, R.A., Schuetz, M., Roach, M., Mansfield, S.D., Ellis, B., and Samuels, L. (2013). Neighboring parenchyma cells contribute to Arabidopsis xylem lignification, while lignification of interfascicular fibers is cell autonomous. Plant Cell **25**: 3988–3999.

Street, P.F.S., Robb, J., and Ellis, B.E. (1986). Secretion of vascular coating components by xylem parenchyma cells of tomatoes infected with *Verticillium albo-atrum*. Protoplasma **132**: 1–11.

Thoquet, P., Olivier, J., Sperisen, C., Rogowsky, P., Laterrot, H., and Grimsley, N. (1996). Quantitative trait loci determining resistance to bacterial wilt in tomato cultivar Hawaii7996. Mol. Plant-Microbe Interact. **9**: 826–836.

Türker-Kaya, S. and Huck, C.W. (2017). A review of mid-infrared and near-infrared imaging: principles, concepts and applications in plant tissue analysis. Molecules **22**: 168.

Underwood, W. (2012). The plant cell wall: a dynamic barrier against pathogen invasion. Front. Plant Sci. **3**: 85.

Ursache, R. *et al.* (2021). GDSL-domain proteins have key roles in suberin polymerization and degradation. Nat. Plants **7**: 353–364.

VanderMolen, G.E., Beckman, C.H., and Rodehorst, E. (1987). The ultrastructure of tylose formation in resistant banana following inoculation with *Fusarium oxysporum*

f.sp. *cubense*. Physiol. Mol. Plant Pathol. **31**: 185–200.

Vasse, J., Frey, P., and Trigalet, A. (1995). Microscopic studies of intercellular infection and protoxylem invasion of tomato roots by *Pseudomonas solanacearum*. Mol. Plant-Microbe Interact. **8**: 241–251.

Vasse, J., Genin, S., Frey, P., Boucher, C., and Brito, B. (2000). The hrpB and hrpG regulatory genes of *Ralstonia solanacearum* are required for different stages of the tomato root infection process. Mol. Plant-Microbe Interact. **13**: 259–267.

Wang, J.F., Ho, F.I., Truong, H.T.H., Huang, S.M., Balatero, C.H., Dittapongpitch, V., and Hidayati, N. (2013). Identification of major QTLs associated with stable resistance of tomato cultivar "Hawaii 7996" to *Ralstonia solanacearum*. Euphytica **190**: 241–252.

Wang, J.F., Olivier, J., Thoquet, P., Mangin, B., Sauviac, L., and Grimsley, N.H. (2000). Resistance of tomato line Hawaii7996 to *Ralstonia solanacearum* Pss4 in Taiwan is controlled mainly by a major strain-specific locus. Mol. Plant-Microbe Interact. **13**: 6–13.

Xu, L., Zhu, L., Tu, L., Liu, L., Yuan, D., Jin, L., Long, L., and Zhang, X. (2011). Lignin metabolism has a central role in the resistance of cotton to the wilt fungus *Verticillium dahliae* as revealed by RNA-seq-dependent transcriptional analysis and histochemistry. J. Exp. Bot. **62**: 5607–5621.

Yadeta, K.A. and Thomma, B.P.H.J. (2013). The xylem as battleground for plant hosts and vascular wilt pathogens. Front. Plant Sci. **4**: 97.

Zeiss, D.R., Mhlongo, M.I., Tugizimana, F., Steenkamp, P.A., and Dubery, I.A. (2019). Metabolomic profiling of the host response of tomato (*Solanum lycopersicum*) following infection by *Ralstonia solanacearum*. Int. J. Mol. Sci. **20**: 3945.

Zeiss, D.R., Piater, L.A., and Dubery, I.A. (2021). Hydroxycinnamate amides: intriguing conjugates of plant protective metabolites. Trends Plant Sci. **26**: 184–195..

Zhang, L., Merlin, I., Pascal, S., Bert, P.F., Domergue, F., and Gambetta, G.A. (2020). Drought activates MYB41 orthologs and induces suberization of grapevine fine roots. Plant Direct **4**: 278

Zhang, Y., Zhang, W., Han, L., Li, J., Shi, X., Hikichi, Y., and Ohnishi, K. (2019). Involvement of a PadR regulator PrhP on virulence of *Ralstonia solanacearum* by

controlling detoxification of phenolic acids and type III secretion system. Mol. Plant Pathol. **20**: 1477–1490.

Zuluaga, A.P., Solé, M., Lu, H., Góngora-Castillo, E., Vaillancourt, B., Coll, N., Buell, C.R., and Valls, M. (2015). Transcriptome responses to *Ralstonia solanacearum* infection in the roots of the wild potato *Solanum commersonii*. BMC Genomics **16**: 246.

Supplemental data:

Table S1: List of primers used in this study.

Table S2: Assignments of the correlation signals in the 2D HSQC spectra.

Figure S1: Tissue used for analysis and bacterial dynamics.

Figure S2: H7996 plants show mild symptoms upon challenge inoculation of *R. solanacearum.*

Figure S3: Vascular coating response to *R. solanacearum* infection with wall bound phenolics.

Figure S4: Expression of suberin biosynthetic genes in xylem vasculature of taproots upon infection of *R. solanacearum*.

Figure S5: Phylogeny of Feruloyl transferase (FHT) orthologues in different plant species and expression of the putative tomato FHT ortholog in response to *Ralstonia solanacearum* infection.

Figure S6: Phylogeny of tyramine hydroxycinnamoyl transferase (THT) orthologues in different plant species and expression of the tomato THT gene family members in response to *R. solanacearum* infection.

Figure S7: Expression of phenylpropanoid pathway genes in xylem vasculature of taproots upon invasion of *R. solanacearum*.

Figure S8: Immunoblot of *35S::SlFHT-HA* in independent Marmande tomato lines expressing *35S::SlFHT-HA* (Marmande).

Figure S9: Fresh weight of *35S::SlFHT-HA* plants.

Figure S10: Fresh weight of *35S::SlTHT1-3* plants.

Figure S11: Overexpression of *SlTHT1-3* in tomato results in restricted colonization by *R. solanacearum*.

Figure Legends

Figure 1: Resistant H7996 tomato restricts *Ralstonia solanacearum* colonization and induces a vascular coating response with wall bound phenolics. Susceptible (Marmande) and resistant (H7996), 5-week old tomato plants were inoculated through roots by soil-soak with ~1x10^7 colony forming units (CFU)/ml of *R. solanacearum* GMI1000 and incubated at 28°C. **(a)** At 12 days post-inoculation (dpi) most Marmande plants showed severe wilting symptoms, whereas H7996 remained mostly symptomless. **(b)** Cross-sections of the taproot-to-hypocotyl area containing 10^5 CFU g^{-1} of *R. solanacearum* were analyzed by ultraviolet (UV) microscopy. To focus on cell wall-deposited phenolic compounds, soluble phenolic compounds were removed with ethanol prior to observation. A strong autoflorescence signal emitted from the walls of vessels and surrounding parenchyma cells in infected H7996 plants compared to Marmande or the mock controls can be observed. Fluorescence signal in white was green colored. Images from a representative experiment out of 3 with *n*=5 plants per cultivar. Scale bar = 500 µm. **(c)** The UV auto-fluorescence signal in (b) was measured using the Leica Application Suite X (LAS X) software. A representative region of interest (ROI) is highlighted in (b) and corresponded to a line traversing the selected vascular bundles. Data are represented with box and whiskers plots: whiskers indicate variability outside the upper and lower quartiles and boxes indicate second quartile, median and third quartile. Different letters indicate statistically significant differences (α=0.05, Fisher's least significant difference test).

Figure 2: Feruloylamides, tyramine-derived amides and suberin-compatible compounds are specifically enriched in resistant H7996 tomato after infection with *R. solanacearum*. (a) Two dimensional heteronuclear single-quantum correlation–nuclear magnetic resonance (2D-HSQC NMR) spectra of enzymatically isolated lignin/suberin fractions from mock-treated and *R. solanacearum*-infected taproots (containing 10^5 CFU g^{-1} taproot-to-hypocotyl transition tissue) of H7996 and Marmande tomato plants. The

experiment was performed twice with similar results. **(b)** Main lignin/suberin structures identified: β–*O*–4′ alkyl aryl ethers (A), β–5′ fenylcoumarans (B), β–β′ resinols (C), cinnamyl alcohols end-groups (I), feruloylamides (FAm), tyramine-derived amides (Ty), guaiacyl lignin units (G), syringyl lignin units (S), as well as unassigned aliphatic signals from suberin. The structures and contours of the HSQC signals are color coded to aid interpretation. ^{1}H and ^{13}C NMR chemical shifts of the assigned signals are detailed in Table S2. To detect FAm_7 signal, the spectrum scaled-up to 2-fold (×2) intensity. The abundances of the main lignin linkages (A, B and C) and cinnamyl alcohol end-groups (I) are referred to as a percentage of the total lignin units (S + G = 100%).

Figure 3: Resistant H7996 tomato shows vascular autofluorescence not-quenched with phloroglucinol and susceptible Marmande shows a decrease in phloroglucinol-HCl lignin signal. Susceptible (Marmande) and resistant (H7996) 5-week-old tomato plants were root-inoculated with a *R. solanacearum* GMI1000 strain at a concentration of ~$1x10^7$ CFU/ml or water mock. **(a)** Cross-sections of the taproot-to-hypocotyl area containing 10^5 CFU g^{-1} of *R. solanacearum* were stained with phloroglucinol-HCl and observed under UV to visualize other autofluorescent compounds different from lignin (not quenched with phloroglucinol-HCl) (right) and under brightfield to visualize lignin deposition (left). In infected H7996 strong UV autofluorescence could be observed in the walls of xylem vessels surrounding xylem parenchyma cells and tracheids, indicating reinforcement of walls of vascular tissue with phenolics formed *de novo* upon infection. In infected Marmande the red phlorogucinol stain was reduced especially in the intervessel areas. **(b)** The UV auto-fluorescence signal in (a) was measured using the LAS X Leica software after the Phloroglucinol-HCl treatment. Data are represented with box and whiskers plots: whiskers indicate variability outside the upper and lower quartiles and boxes indicate second quartile, median and third quartile. **(c)** Detailed observation of infected H7996 xylem after the Phloroglucinol-HCl treatment shows the strong UV fluorescence concentrated in specific areas possibly corresponding to intervessel and vessel-parenchyma bordered pit membranes and/or pit chambers (yellow and white arrows, respectively). Fluorescence was also observed in parenchyma cells, specially enriched at intercellular cell corners (green arrow). (b) correspond to a representative experiment out of 3 each with n=6

plants per variety. Different letters indicate statistically significant differences (α=0.05, Fisher's least significant difference test). (a) and (c) were representative images. Scale bars = 100 μm in (a, left), 500 μm in (a, right) and 50 μm in (c).

Figure 4: Resistant H7996 tomato shows cell wall ferulate/feruloylamide and suberin deposition in restricted zones of vascular tissue upon *R. solanacearum* infection. Susceptible Marmande or resistant H7996 tomato plants were soil-inoculated with a ~1x10^7 CFU/ml suspension of *Ralstonia solanacearum* GMI1000 or mock-inoculated with water and incubated at 28°C. Cross-sections were obtained from taproot-to-hypocotyl transition tissue containing 10^5 CFU g^{-1} of *R. solanacearum*. Sections were stained with Sudan IV to visualize suberin aliphatics and subsequently treated with 1N KOH (pH above 10) to visualize ferulic acid bound to cell wall. Sudan IV positive staining (reddish-brown coloration) was observed around xylem vessels specifically in infected H7996, indicating accumulation of suberin aliphatics. Accumulation of ferulic acid bound to cell wall (blue-green coloration) appears also specifically in infected H7996 resistant tomato, surrounding Sudan IV-stained areas. White arrowheads indicate the sites of accumulation of ferulates and aliphatic compounds. Representative images from one experiment out of three with *n*=6 plants each were taken. Scale bar= 100 μm.

Figure 5: Genes of the ligno-suberin heteropolymer biosynthesis pathway are specifically induced in the xylem vasculature of resistant H7996 tomato upon *R. solanacearum* infection. The levels of expression of genes belonging to metabolic pathways relevant for suberin, lignin and feruloyltyramine and related amides biosynthesis were analyzed by quantitative PCR (qPCR) of taproot vascular tissue in infected or mock-treated H7996 or Marmande tomato plants. Plants containing an *R. solanacearum* inoculum of 10^5 CFU g^{-1} were selected and xylem vascular tissue from the taproot-to-hypocotyl transition zone, comprising of metaxylems and surrounding parenchyma cells was collected for RNA extraction and cDNA synthesis. In parallel, xylem tissue was collected from mock plants. Heatmaps show $\log_2$ fold change RTA (relative transcript abundance) values of infected vs. mock for Marmande (left) and Hawaii (right). The tomato gene encoding for the alpha-subunit of the translation elongation factor 1 (*SleEF1 α*) was used as endogenous

reference. Three biological replicates (n=3) were used, and taproots of 6 plants were used in each replicate. All the original qPCR results can be found in Figs. S3, S4, S5 and S6. The scheme represents the phenylpropanoid and suberin biosynthesis pathways providing lignin-like and suberin precursors for the ligno-suberin heteropolymer. Abbreviations: PAL: Phenylalanine ammonia–lyase; C4H: Cinnamate–4–hydroxylase; C3H: Coumarate 3-hydroxylase; 4CL: 4–Coumarate–CoA ligase; HCT: Hydroxycinnamoyl–CoA shikimate/quinate hydroxycinnamoyl transferase; COMT: Caffeic acid 3-O-methyltransferase; CCoAOMT: Caffeoyl CoA 3-O-methyltransferase; CYP86A1 and CYP86B1: cytochrome P450 fatty acid ω-hydroxylases; KCS1/2: 3-ketoacyl-CoA synthase; FAR 1/3/4: Fatty acyl-CoA reductase; GPAT5: glycerol-3-phosphate acyltransferase 5; THT: Tyramine hydroxycinnamoyl transferase; TyDC: Tyrosine decarboxylase; FHT: feruloyl transferase. The question mark (?) denotes a hypothetical reaction.

Figure 6: Overexpression of *SlFHT-HA* in susceptible tomato slightly restricts colonization by *R. solanacearum*. (a, b) A pathogenicity assay was performed comparing Wt and 3 independent *35S::SlFHT-HA* Marmande tomato lines (a, c and d) after infection with *R. solanacearum* GMI1000 lux reporter strain. Five-week-old plants were soil-soak inoculated with ~1x10^7 CFU/ml or mock and grown at 28°C. **(a)** Wilting progress was monitored by rating plants daily on a 0 to 4 disease index scale where 0 = healthy and 4 =100% wilted. Plotted values correspond to means ± standard error of 24 independent plants (n=24) from a representative experiment out of a total of 3. Asterisks indicate statistically significant differences between Wt and each of the *35S::FHT-HA* analyzed using a paired Student's t-test (* $p<0.05$). **(b)** The level of *R. solanacearum* colonization in the taproot and hypocotyl was calculated as colony forming units per gram of fresh taproot tissue (CFU·g^{-1}) at 12 dpi. Data are represented with box and whiskers plots: whiskers indicate variability outside the upper and lower quartiles and boxes indicate second quartile, median and third quartile. Data presented are of a representative experiment out of a total of 3 experiments. In (a) a Kruskall-Wallis test at each day post infection (dpi) was conducted to examine differences in disease index among different genotypes. Significant differences among genotypes were confirmed by applying a pairwise Wilcox test. Asterisks

indicate statistically significant differences between wild type and *35S::FHT-HA* tomato lines in a (* corresponds to a p-value of $p < 0.05$).

Figure 7: Overexpression of *SlTHT1-3* in susceptible tomato confers resistance to *R. solanacearum*. (a, b) A pathogenicity assay was performed comparing Wt and *35S::SlTHT1-3* tomato lines (Moneymaker background) after infection with *R. solanacearum* lux reporter GMI1000 strain. Five-week-old plants were soil-soak inoculated with ~$1x10^7$ CFU/ml and grown at 28°C. **(a)** Wilting progress was monitored by rating plants daily on a 0 to 4 disease index scale where 0 = healthy and 4 =100% wilted. Plotted values correspond to means ± standard error of 24 independent plants (n=24) from a representative experiment out of a total of 3. Asterisks indicate statistically significant differences between Wt and *35S::SlTHT1-3* using a Kruskall-Wallis test at each day post infection (dpi) was conducted to examine differences in disease index among different genotypes. Significant differences among genotypes were confirmed by applying a pairwise Wilcox test". (* corresponds to a p-value of $p < 0.05$ and *** to $p < 0.0001$). **(b)** Pictures were taken 12 days post-infection. Wt plants were arranged according to the degree of symptom severity (from 4 to 0). **(c)** Transgenic *35S::SlTHT1-3* tomato significantly restricted *R. solanacearum* colonization in both the taproot-to-hypocotyl transition zone and hypocotyl compared to Wt. Five-week-old tomato plants were root-inoculated with a *R. solanacearum* GMI1000 luciferase reporter strain at a concentration of ~$1x10^7$ CFU/ml or water mock. The level of *in planta* colonization by *R. solanacearum* was calculated as colony forming units per gram of fresh taproot tissue ($CFU \cdot g^{-1}$) at 12 dpi. Data are represented with box and whiskers plots: whiskers indicate variability outside the upper and lower quartiles and boxes indicate second quartile, median and third quartile. Box-and-whisker plots show data from a representative experiment out of 3 (n =14 to 16). (*** corresponds to a p-value of $p < 0.0001$) **(d)** Transverse stem cross-sections of Wt and transgenic *35S::SlTHT1-3* tomato lines were imaged under a confocal microscope 6 days after infection with a *R. solanacearum* GMI1000 green fluorescent protein (GFP) reporter strain. *R. solanacearum* at a concentration of 10^5 CFU ml^{-1} was injected directly into the xylem vasculature of the first internode thorough the petiole. Orange arrow points the site of inoculation. Representative images of *R. solanacearum* colonization progress at the point

of inoculation are shown. Scale bar= 2 mm. **(e)** Mean green fluorescence of the GFP signal emitted from *R. solanacearum* at cross-sections obtained as described in (d) at the point of inoculation (0), below the point of inoculation (-0.5 cm) and above the point of inoculation (+0.5 cm) was measured using ImageJ. Data are represented with box and whiskers plots: whiskers indicate variability outside the upper and lower quartiles and boxes indicate second quartile, median and third quartile. Data from a representative experiment out of a total of 3, with *n*=5 plants per condition. In (a) a Kruskall-Wallis test at each day post infection (dpi) was conducted to examine differences in disease index among different genotypes. Significant differences among genotypes were confirmed by applying a pairwise Wilcox test. Asterisks indicate statistically significant differences between wild type and *35S::SlTHT1-3* tomato lines in (a) (* corresponds to a p-value of $p < 0.05$ and ** to $p < 0.001$).

Figure 8: Overexpression of *SlTHT1-3* in susceptible tomato results in vascular autofluorescence not-quenched with phloroglucinol and cell wall ferulate/feruloylamide deposition in restricted zones of vascular tissue upon *R. solanacearum* infection. Susceptible Moneymaker (Wt) or resistant *35S::SlTHT1-3* overxpressing tomato plants were soil-inoculated with a ~$1x10^7$ CFU/ml suspension of *R. solanacearum* GMI1000 lux reporter strain. Cross-sections were obtained from taproot-to-hypocotyl of both genotypes tissue containing containing 10^5 CFU g^{-1} of *R. solanacearum*. **(a)** Cross-sections were stained with phloroglucinol-HCl and observed under brightfield to visualize lignin deposition (left) and under UV to visualize other auto-fluorescent compounds different from lignin (not quenched with phloroglucionol- HCl) (right). **(b)** Combined Sudan IV+KOH treatment showed no positive suberin aliphatic signal in *SlTHT1-3*, but a significant increase in ferulate/feruloylamide accumulation upon infection. **(c)** Close-ups (10X) of the vascular bundles of Wt and *35S::SlTHT1-3* infected plants pointed with a white arrow in (b) are also shown. Images from a representative experiment out of 3 with n=6 plants per cultivar. **(d)** Quantification of UV fluorescence after phloroglucinol-HCl staining as shown in (a, right) were performed with LAS X software by selecting the vascular areas surrounding main vessels with strong localized fluorescence or green signal. **(e)** Quantification of UV green fluorescence from ferulate deposits after

Sudan IV+KOH staining as shown in (a, right) were performed with LAS X software by selecting the vascular areas surrounding main vessels with strong localized fluorescence or green signal. Data in (d) and (e) are represented with box and whiskers plots: whiskers indicate variability outside the upper and lower quartiles and boxes indicate second quartile, median and third quartile. Different letters indicate statistically significant differences (α=0.05, Fisher's least significant difference test). Scale bar = 500 μm.

Figure 9: Schematic representation of the vascular ligno-suberization process potentially taking place in infected vessels of resistant H7996 tomato upon *R. solanacearum* infection. Colonization of the vasculature by *R. solanacearum* in resistant tomato plants induces a ligno-suberization process in the walls of the infected vessel (V) and of the adjacent tracheids (T) and parenchyma cells (XP) (red). The lignin-like polymer accompanying suberin would be enriched in structural feruloyltyramine and related amides. The signal of structural ferulic acid (ester or as amide) would extend to the walls of peripheral parenchyma cells, vessels and tracheids (green), indicating a stage preceding suberization or a final layered pattern, still to be resolved. Together, the red and green areas, would form a "zone of ligno-suberization" (black dashed line) potentially creating a physico-chemical barrier to limit *R. solanacearum* spread from the colonized xylem vessel lumen.

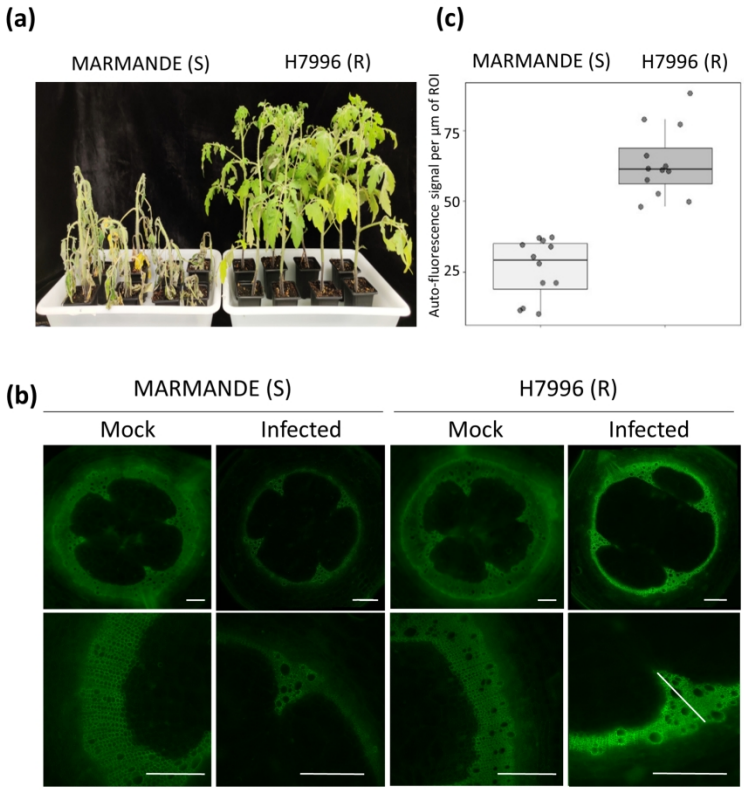

FIGURE 1

Figure 1: Resistant H7996 tomato restricts Ralstonia solanacearum colonization and induces a vascular coating response with wall bound phenolics. Susceptible (Marmande) and resistant (H7996), 5-week old tomato plants were inoculated through roots by soil-soak with ~1x107 colony forming units (CFU)/ml of R. solanacearum GMI1000 and incubated at 28°C. (a) At 12 days post-inoculation (dpi) most Marmande plants showed severe wilting symptoms, whereas H7996 remained mostly symptomless. (b) Cross-sections of the taproot-to-hypocotyl area containing 105 CFU g −1 of R. solanacearum were analyzed by ultraviolet (UV) microscopy. To focus on cell wall-deposited phenolic compounds, soluble phenolic compounds were removed with ethanol prior to observation. A strong autoflorescence signal emitted from the walls of vessels and surrounding parenchyma cells in infected H7996 plants compared to Marmande or the mock controls can be observed. Fluorescence signal in white was green colored. Images from a representative experiment out of 3 with n=5 plants per cultivar. Scale bar = 500 µm. (c) The UV auto-fluorescence signal in (b) was measured using the Leica Application Suite X (LAS X) software. A representative region of interest (ROI) is highlighted in (b) and corresponded to a line traversing the selected vascular bundles. Data are represented with box and whiskers plots: whiskers indicate variability outside the upper and lower quartiles and boxes indicate

second quartile, median and third quartile. Different letters indicate statistically significant differences (α=0.05, Fisher's least significant difference test).

561x810mm (96 x 96 DPI)

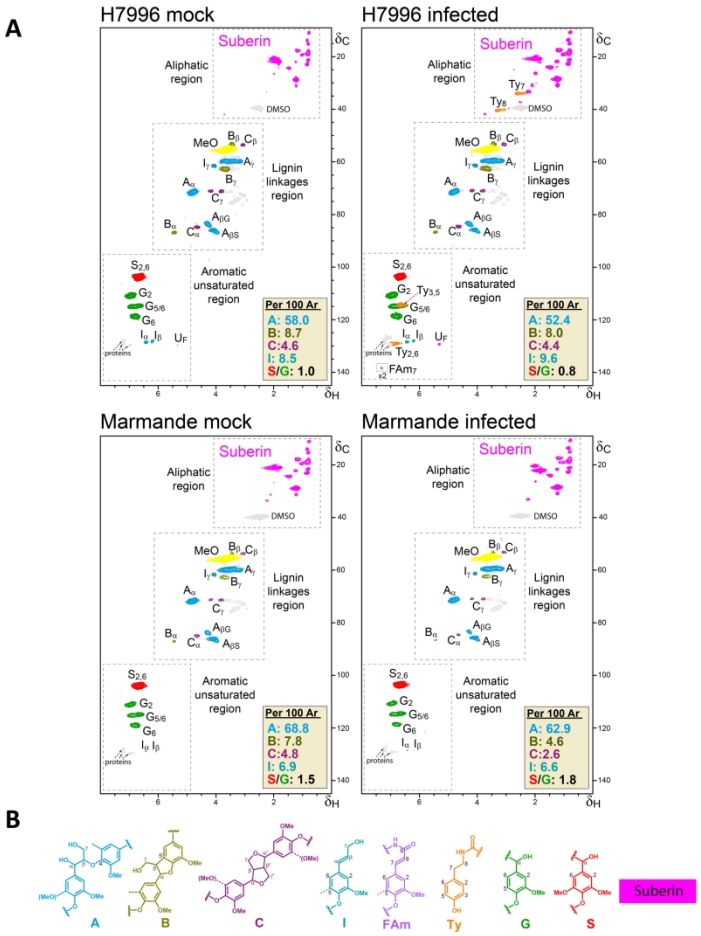

Figure 2: Feruloylamides, tyramine-derived amides and suberin-compatible compounds are specifically enriched in resistant H7996 tomato after infection with R. solanacearum. (a) 2D-HSQC NMR spectra of enzymatically isolated lignin/suberin fractions from mock-treated and R. solanacearum-infected taproots (containing 105 CFU g-1 taproot-to-hypocotyl transition tissue) of H7996 and Marmande tomato plants. The experiment was performed twice with similar results. (b) Main lignin/suberin structures identified: β–O–4′ alkyl aryl ethers (A), β–5′ fenylcoumarans (B), β–β′ resinols (C), cinnamyl alcohols end-groups (I), feruloylamides (FAm), tyramine-derived amides (Ty), guaiacyl lignin units (G), syringyl lignin units (S), as well as unassigned aliphatic signals from suberin. The structures and contours of the HSQC signals are color coded to aid interpretation. 1H and 13C NMR chemical shifts of the assigned signals are detailed in Table S1. To detect FAm7 signal, the spectrum scaled-up to 2-fold (×2) intensity. The abundances of the main lignin linkages (A, B and C) and cinnamyl alcohol end-groups (I) are referred to as a percentage of the total lignin units (S + G = 100%).

248x244mm (300 x 300 DPI)

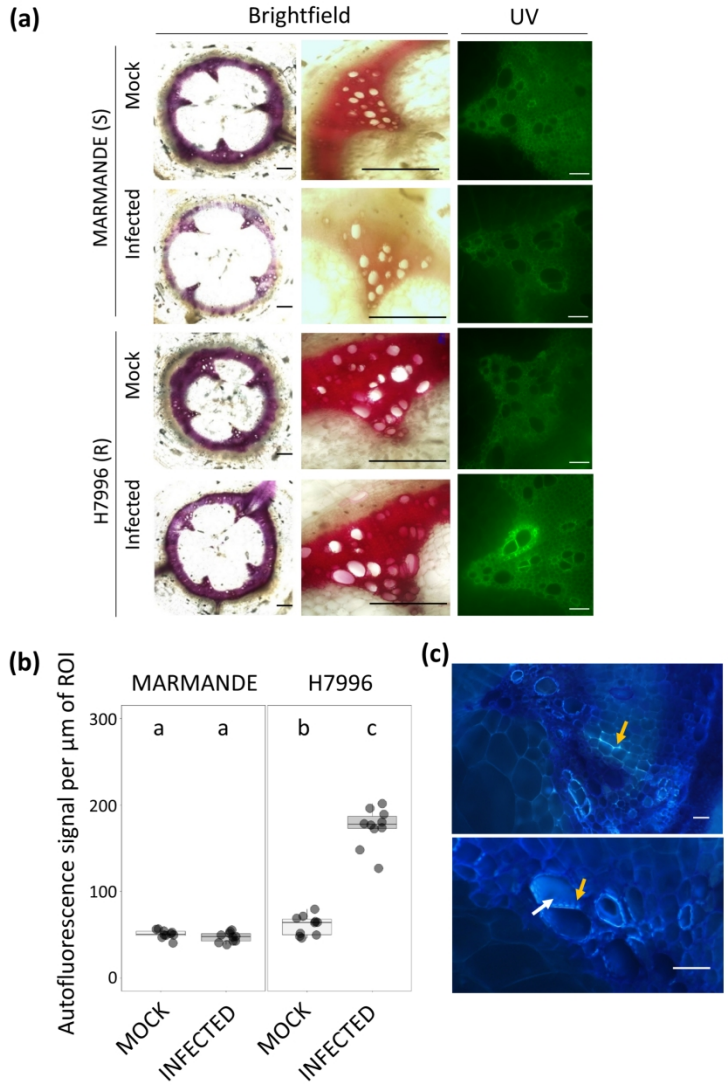

FIGURE 3

Figure 3: Resistant H7996 tomato shows vascular autofluorescence not-quenched with phloroglucinol and susceptible Marmande shows a decrease in phloroglucinol-HCl lignin signal. Susceptible (Marmande) and resistant (H7996) 5-week-old tomato plants were root-inoculated with a R. solanacearum GMI1000 strain at a concentration of ~1x107 CFU/ml or water mock. (a) Cross-sections of the taproot-to-hypocotyl area containing 105 CFU g −1 of R. solanacearum were stained with phloroglucinol-HCl and observed under UV to visualize other autofluorescent compounds different from lignin (not quenched with phloroglucinol-HCl) (right) and under brightfield to visualize lignin deposition (left). In infected H7996 strong UV autofluorescence could be observed in the walls of xylem vessels surrounding xylem parenchyma cells and tracheids, indicating reinforcement of walls of vascular tissue with phenolics formed de novo upon infection. In infected Marmande the red phlorogucinol stain was reduced especially in the intervessel areas. (b) The UV auto-fluorescence signal in (a) was measured using the LAS X Leica software after the Phloroglucinol-HCl treatment. Data are represented with box and whiskers plots: whiskers indicate variability outside the upper and lower quartiles and boxes indicate second quartile, median and third quartile. (c) Detailed observation of infected H7996 xylem after the Phloroglucinol-HCl treatment shows the strong UV fluorescence

concentrated in specific areas possibly corresponding to intervessel and vessel-parenchyma bordered pit membranes and/or pit chambers (yellow and white arrows, respectively). Fluorescence was also observed in parenchyma cells, specially enriched at intercellular cell corners (green arrow). (b) correspond to a representative experiment out of 3 each with n=6 plants per variety. Different letters indicate statistically significant differences (α=0.05, Fisher's least significant difference test). (a) and (c) were representative images. Scale bars = 100 μm in (a, left), 500 μm in (a, right) and 50 μm in (c).

190x275mm (283 x 283 DPI)

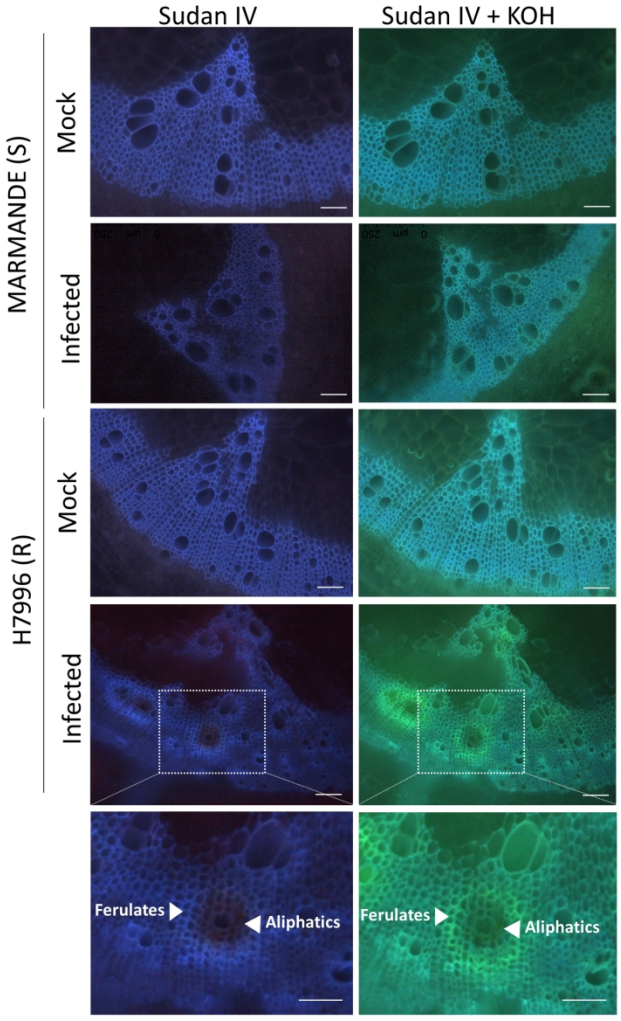

FIGURE 4

Figure 4: Resistant H7996 tomato shows cell wall ferulate/feruloylamide and suberin deposition in restricted zones of vascular tissue upon R. solanacearum infection. Susceptible Marmande or resistant H7996 tomato plants were soil-inoculated with a ~1x107 CFU/ml suspension of Ralstonia solanacearum GMI1000 or mock-inoculated with water and incubated at 28°C. Cross-sections were obtained from taproot-to-hypocotyl transition tissue containing 105 CFU g −1 of R. solanacearum. Sections were stained with Sudan IV to visualize suberin aliphatics and subsequently treated with 1N KOH (pH above 10) to visualize ferulic acid bound to cell wall. Sudan IV positive staining (reddish-brown coloration) was observed around xylem vessels specifically in infected H7996, indicating accumulation of suberin aliphatics. Accumulation of ferulic acid bound to cell wall (blue-green coloration) appears also specifically in infected H7996 resistant tomato, surrounding Sudan IV-stained areas. White arrowheads indicate the sites of accumulation of ferulates and aliphatic compounds. Representative images from one experiment out of three with n=6 plants each were taken. Scale bar= 100 µm.

190x275mm (283 x 283 DPI)

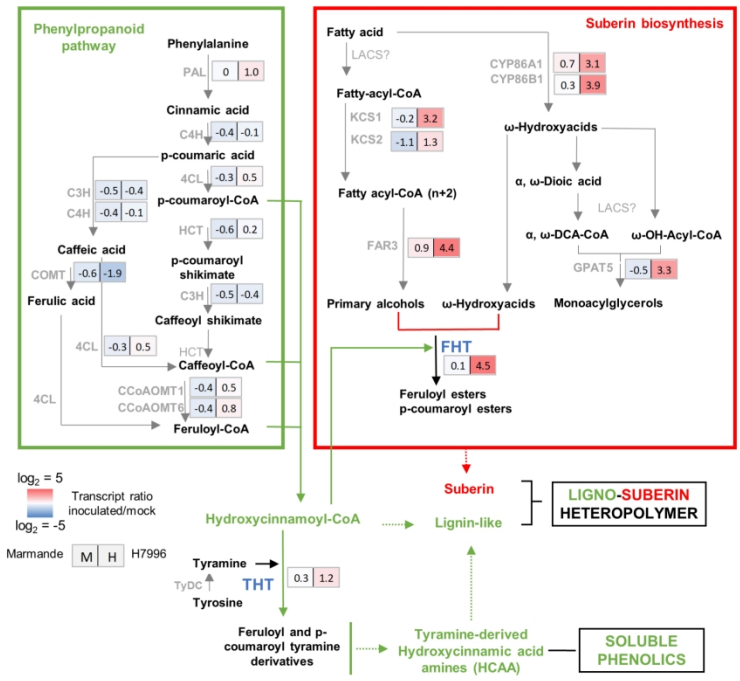

FIGURE 5

Figure 5: Genes of the ligno-suberin heteropolymer biosynthesis pathway are specifically induced in the xylem vasculature of resistant H7996 tomato upon R. solanacearum. The levels of expression of genes belonging to metabolic pathways relevant for suberin, lignin and feruloyltyramine and related amides biosynthesis were analyzed by qPCR of taproot vascular tissue in infected or mock-treated H7996 or Marmande tomato plants. Plants containing an R. solanacearum inoculum of 105 CFU g−1 were selected and xylem vascular tissue from the taproot-to-hypocotyl transition zone, comprising of metaxylems and surrounding parenchyma cells was collected for RNA extraction and cDNA synthesis. In parallel, xylem tissue was collected from mock plants. Heatmaps show log2 fold change RTA (relative transcript abundance) values of infected vs. mock for Marmande (left) and Hawaii (right). The tomato gene encoding for the alpha-subunit of the translation elongation factor 1 (SleEF1 α) was used as endogenous reference. Three biological replicates (n=3) were used, and taproots of 6 plants were used in each replicate. All the original qPCR results can be found in Figs. S3, S4, S5 and S6. The scheme represents the phenylpropanoid and suberin biosynthesis pathways providing lignin-like and suberin precursors for the ligno-suberin heteropolymer. Abbreviations: PAL: Phenylalanine ammonia–lyase; C4H: Cinnamate–4–hydroxylase; C3H: Coumarate 3-

hydroxylase; 4CL: 4–Coumarate–CoA ligase; HCT: Hydroxycinnamoyl–CoA shikimate/quinate hydroxycinnamoyl transferase; COMT: Caffeic acid 3-O-methyltransferase; CCoAOMT: Caffeoyl CoA 3-O-methyltransferase; CYP86A1 and CYP86B1: cytochrome P450 fatty acid ω-hydroxylases; KCS1/2: 3-ketoacyl-CoA synthase; FAR 1/3/4: Fatty acyl-CoA reductase; GPAT5: glycerol-3-phosphate acyltransferase 5; THT: Tyramine hydroxycinnamoyl transferase; TyDC: Tyrosine decarboxylase; FHT: feruloyl transferase. The question mark (?) denotes a hypothetical reaction.

190x275mm (283 x 283 DPI)

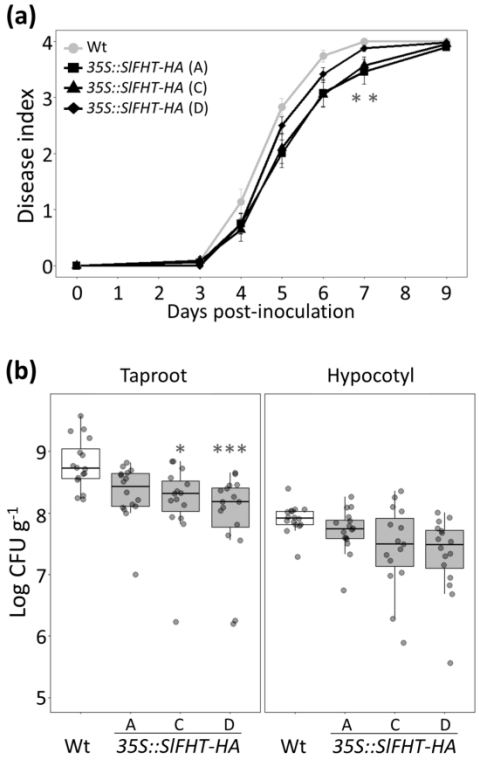

FIGURE 6

Figure 6: Overexpression of SlFHT-HA in susceptible tomato slightly restricts colonization by R. solanacearum. (a, b) A pathogenicity assay was performed comparing Wt and 3 independent 35S::SlFHT-HA Marmande tomato lines (a, c and d) after infection with R. solanacearum GMI1000 lux reporter strain. Five-week-old plants were soil-soak inoculated with ~1x107 CFU/ml or mock and grown at 28°C. (a) Wilting progress was monitored by rating plants daily on a 0 to 4 disease index scale where 0 = healthy and 4 =100% wilted. Plotted values correspond to means ± standard error of 24 independent plants (n=24) from a representative experiment out of a total of 3. Asterisks indicate statistically significant differences between Wt and each of the 35S::FHT-HA analyzed using a paired Student's t-test (* $p<0.05$). (b) The level of R. solanacearum colonization in the taproot and hypocotyl was calculated as colony forming units per gram of fresh taproot tissue (CFU·g −1) at 12 dpi. Data are represented with box and whiskers plots: whiskers indicate variability outside the upper and lower quartiles and boxes indicate second quartile, median and third quartile. Data presented are of a representative experiment out of a total of 3 experiments. In (a) a Kruskall-Wallis test at each day post infection (dpi) was conducted to examine differences in disease index among different genotypes. Significant differences among genotypes were confirmed by applying a pairwise

Wilcox test. Asterisks indicate statistically significant differences between wild type and 35S::FHT-HA tomato lines in a (* corresponds to a p-value of $p < 0.05$).

190x275mm (283 x 283 DPI)

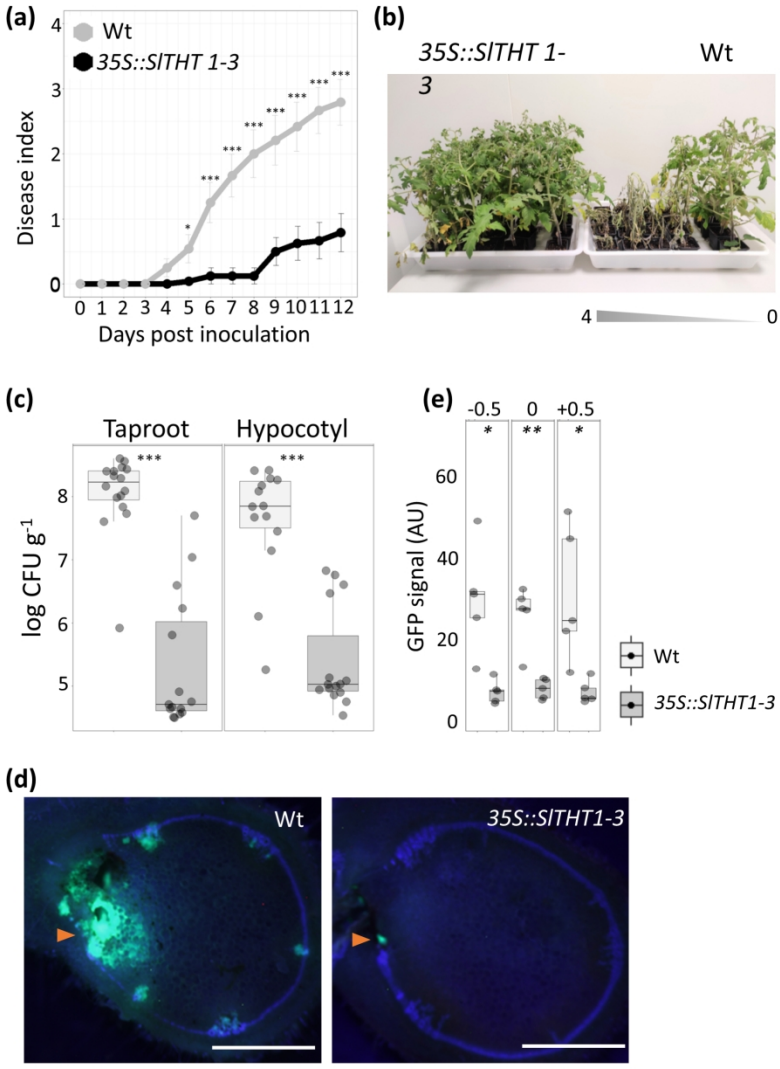

FIGURE 7

Figure 7: Overexpression of SlTHT1-3 in susceptible tomato confers resistance to R. solanacearum. (a, b) A pathogenicity assay was performed comparing Wt and 35S::SlTHT1-3 tomato lines (Moneymaker background) after infection with R. solanacearum lux reporter GMI1000 strain. Five-week-old plants were soil-soak inoculated with ~1x107 CFU/ml and grown at 28°C. (a) Wilting progress was monitored by rating plants daily on a 0 to 4 disease index scale where 0 = healthy and 4 =100% wilted. Plotted values correspond to means ± standard error of 24 independent plants (n=24) from a representative experiment out of a total of 3. Asterisks indicate statistically significant differences between Wt and 35S::SlTHT1-3 using a Kruskall-Wallis test at each day post infection (dpi) was conducted to examine differences in disease index among different genotypes. Significant differences among genotypes were confirmed by applying a pairwise Wilcox test". (* corresponds to a p-value of $p < 0.05$ and *** to $p < 0.0001$). (b) Pictures were taken 12 days post-infection. Wt plants were arranged according to the degree of symptom severity (from 4 to 0). (c) Transgenic 35S::SlTHT1-3 tomato significantly restricted R. solanacearum colonization in both the taproot-to-hypocotyl transition zone and hypocotyl compared to Wt. Five-week-old tomato plants were root-inoculated with a R. solanacearum GMI1000 luciferase reporter strain at a concentration of ~1x107 CFU/ml

or water mock. The level of in planta colonization by R. solanacearum was calculated as colony forming units per gram of fresh taproot tissue (CFU·g −1) at 12 dpi. Data are represented with box and whiskers plots: whiskers indicate variability outside the upper and lower quartiles and boxes indicate second quartile, median and third quartile. Box-and-whisker plots show data from a representative experiment out of 3 (n =14 to 16). (*** corresponds to a p-value of $p < 0.0001$) (d) Transverse stem cross-sections of Wt and transgenic 35S::SlTHT1-3 tomato lines were imaged under a confocal microscope 6 days after infection with a R. solanacearum GMI1000 green fluorescent protein (GFP) reporter strain. R. solanacearum at a concentration of 105 CFU ml −1 was injected directly into the xylem vasculature of the first internode thorough the petiole. Orange arrow points the site of inoculation. Representative images of R. solanacearum colonization progress at the point of inoculation are shown. Scale bar= 2 mm. (e) Mean green fluorescence of the GFP signal emitted from R. solanacearum at cross-sections obtained as described in (d) at the point of inoculation (0), below the point of inoculation (-0.5 cm) and above the point of inoculation (+0.5 cm) was measured using ImageJ. Data are represented with box and whiskers plots: whiskers indicate variability outside the upper and lower quartiles and boxes indicate second quartile, median and third quartile. Data from a representative experiment out of a total of 3, with n=5 plants per condition. In (a) a Kruskall-Wallis test at each day post infection

190x275mm (283 x 283 DPI)

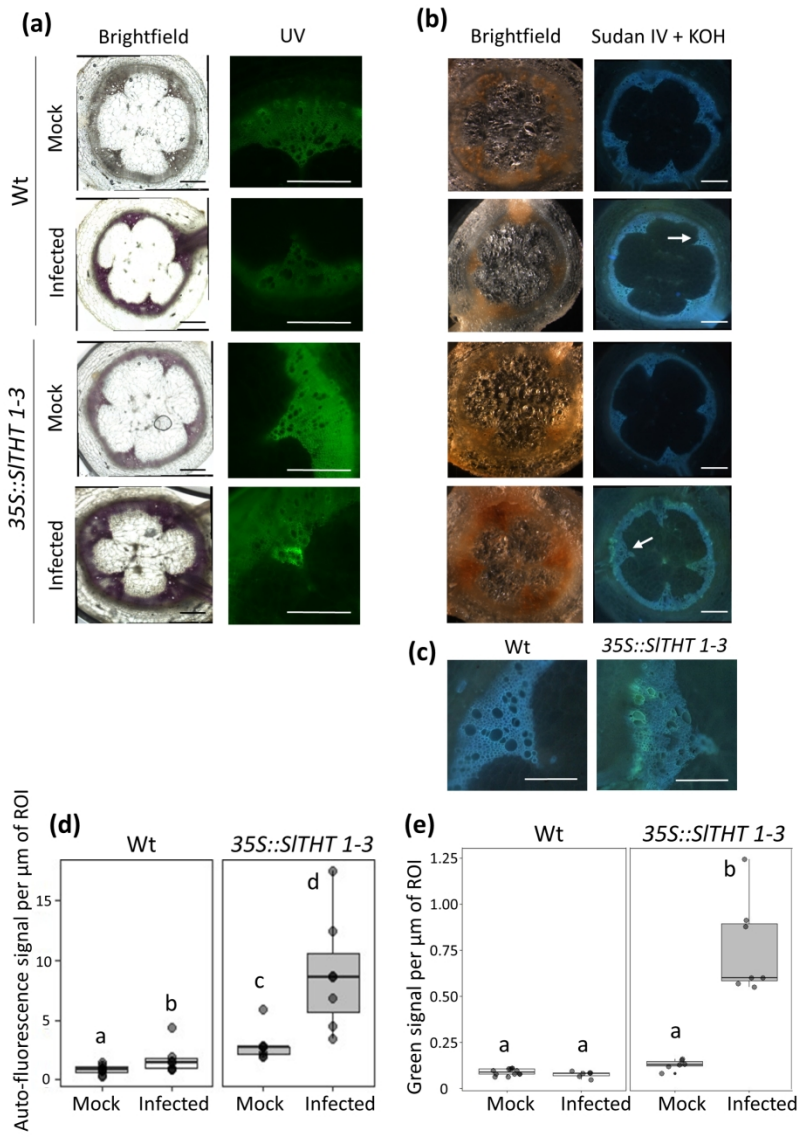

FIGURE 8

Figure 8: Overexpression of SlTHT1-3 in susceptible tomato results in vascular autofluorescence not-quenched with phloroglucinol and cell wall ferulate/feruloylamide deposition in restricted zones of vascular tissue upon R. solanacearum infection. Susceptible Moneymaker (Wt) or resistant 35S::SlTHT1-3 overxpressing tomato plants were soil-inoculated with a ~1x107 CFU/ml suspension of R. solanacearum GMI1000 lux reporter strain. Cross-sections were obtained from taproot-to-hypocotyl of both genotypes tissue containing containing 105 CFU g−1 of R. solanacearum. (a) Cross-sections were stained with phloroglucinol-HCl and observed under brightfield to visualize lignin deposition (left) and under UV to visualize other auto-fluorescent compounds different from lignin (not quenched with phloroglucionol- HCl) (right). (b) Combined Sudan IV+KOH treatment showed no positive suberin aliphatic signal in SlTHT1-3, but a significant increase in ferulate/feruloylamide accumulation upon infection. (c) Close-ups (10X) of the vascular bundles of Wt and 35S::SlTHT1-3 infected plants pointed with a white arrow in (b) are also shown. Images from a representative experiment out of 3 with n=6 plants per cultivar. (d) Quantification of UV fluorescence after phloroglucinol-HCl staining as shown in (a, right) were performed with LAS X software by selecting the vascular areas surrounding main vessels with strong localized fluorescence or green signal. (e)

Quantification of UV green fluorescence from ferulate deposits after Sudan IV+KOH staining as shown in (a, right) were performed with LAS X software by selecting the vascular areas surrounding main vessels with strong localized fluorescence or green signal. Data in (d) and (e) are represented with box and whiskers plots: whiskers indicate variability outside the upper and lower quartiles and boxes indicate second quartile, median and third quartile. Different letters indicate statistically significant differences (α=0.05, Fisher's least significant difference test). Scale bar = 500 µm.

190x275mm (283 x 283 DPI)

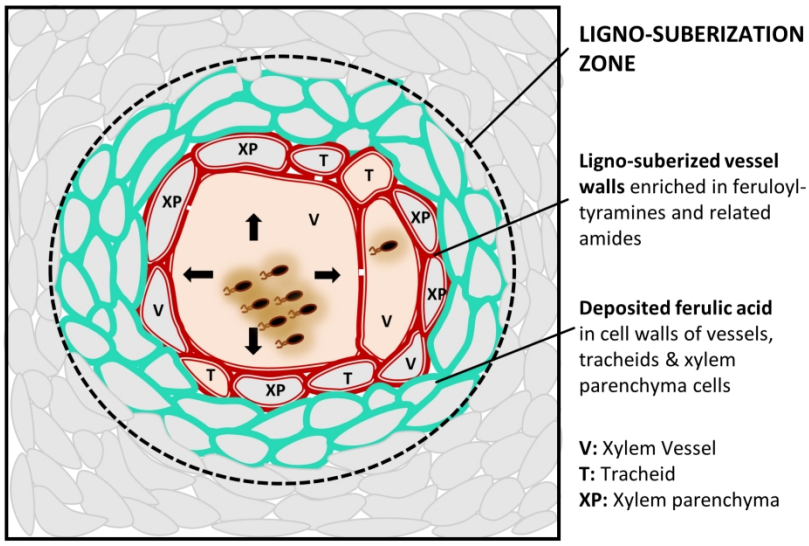

FIGURE 9

Figure 9: Schematic representation of the vascular ligno-suberization process potentially taking place in infected vessels of resistant H7996 tomato upon R. solanacearum infection. Colonization of the vasculature by R. solanacearum in resistant tomato plants induces a ligno-suberization process in the walls of the infected vessel (V) and of the adjacent tracheids (T) and parenchyma cells (XP) (red). The lignin-like polymer accompanying suberin would be enriched in structural feruloyltyramine and related amides. The signal of structural ferulic acid (ester or as amide) would extend to the walls of peripheral parenchyma cells, vessels and tracheids (green), indicating a stage preceding suberization or a final layered pattern, still to be resolved. Together, the red and green areas, would form a "zone of ligno-suberization" (black dashed line) potentially creating a physico-chemical barrier to limit R. solanacearum spread from the colonized xylem vessel lumen.

190x275mm (283 x 283 DPI)